The Journal of Chemical Physics

Consistent schemes for non-adiabatic dynamics derived from partial linearized density matrix propagation

Cite as: J. Chem. Phys. **137**, 22A535 (2012); https://doi.org/10.1063/1.4748316
Submitted: 04 June 2012 . Accepted: 14 August 2012 . Published Online: 04 September 2012

Pengfei Huo, and David F. Coker

Consistent schemes for non-adiabatic dynamics derived from partial linearized density matrix propagation

Pengfei Huo[1,2,a)] and David F. Coker[1,3,a)]
[1]*Department of Chemistry, Boston University, 590 Commonwealth Avenue, Boston, Massachusetts 02215, USA*
[2]*Division of Chemistry and Chemical Engineering, California Institute of Technology, Pasadena, California 91125, USA*
[3]*Department of Physics, and Complex Adaptive Systems Laboratory, University College Dublin, Dublin 4, Ireland*

(Received 4 June 2012; accepted 14 August 2012; published online 4 September 2012)

Powerful approximate methods for propagating the density matrix of complex systems that are conveniently described in terms of electronic subsystem states and nuclear degrees of freedom have recently been developed that involve linearizing the density matrix propagator in the difference between the forward and backward paths of the nuclear degrees of freedom while keeping the interference effects between the different forward and backward paths of the electronic subsystem described in terms of the mapping Hamiltonian formalism and semi-classical mechanics. Here we demonstrate that different approaches to developing the linearized approximation to the density matrix propagator can yield a mean-field like approximate propagator in which the nuclear variables evolve classically subject to Ehrenfest-like forces that involve an average over quantum subsystem states, and by adopting an alternative approach to linearizing we obtain an algorithm that involves classical like nuclear dynamics influenced by a quantum subsystem state dependent force reminiscent of trajectory surface hopping methods. We show how these different short time approximations can be implemented iteratively to achieve accurate, stable long time propagation and explore their implementation in different representations. The merits of the different approximate quantum dynamics methods that are thus consistently derived from the density matrix propagator starting point and different partial linearization approximations are explored in various model system studies of multi-state scattering problems and dissipative non-adiabatic relaxation in condensed phase environments that demonstrate the capabilities of these different types of approximations for treating non-adiabatic electronic relaxation, bifurcation of nuclear distributions, and the passage from nonequilibrium coherent dynamics at short times to long time thermal equilibration in the presence of a model dissipative environment.
 [http://dx.doi.org/10.1063/1.4748316]

I. INTRODUCTION

The mixed quantum-classical strategy for modeling systems in which quantum coherent dynamics and electronically non-adiabatic transitions play important roles describes the nuclear degrees of freedom (DOF) classically or semi-classically, while treating the electronic DOF quantum mechanically with an evolution operator parameterized by trajectories of the nuclear DOF.[1–3]

The two most widely used approaches to mixed quantum-classical dynamics are mean-field based Ehrenfest dynamics schemes,[1,2,4] and the trajectory surface hopping methods.[1,5–8] Ehrenfest dynamics methods propagate the nuclear DOF using a mean-field that employs a time dependent average of different potentials arising from the mixing quantum subsystem states. This mean-field is parameterize by the time dependent electronic expansion coefficients. Surface hopping schemes, on the other hand, evolve the nuclear DOF based on a single electronic adiabatic potential with hops between surfaces determined by a stochastic algorithm and additional impulsive hopping forces arising from the non-adiabatic coupling vector matrix elements that describe the back reaction between the quantum and classical DOF during quantum transitions.[1,5] These forces operate to conserve energy during instantaneous surface hopping events along given trajectories. Though quite successful in many applications treating non-adiabatic dynamics, these two schemes have different disadvantages that result from their different central approximations.

Ehrenfest dynamics, or related mean-field approaches, such as the time dependent self consistent field (TDSCF),[4] or linearized semi-classical initial value representation (LSC-IVR)[9,10] schemes, cannot in general, for example, provide an accurate description of bond breaking process where, once the wave packet emerges from the coupling region where the electronic states mix, the force that acts on the nuclear DOF should be that arising from a single surface potential, rather than the mean force averaged over multiple potentials. Surface hopping methods that branch trajectories between the different competing potential surfaces and integrate the electronic wave function coherently along the classical-like trajectories of the nuclear DOF, partially overcome this problem but require the use of *ad hoc* schemes to deal with the decoherence that arises as nuclear wave packets, born on

a)Electronic addresses: pengfhuo@caltech.edu and coker@bu.edu.

the different surfaces move in different directions and their overlap modulates the off-diagonal coherence density matrix elements.[11] This is due to the fact that trajectory hopping in most surface hopping (SH) methods does not correctly represent the developing independent nature of the bifurcating wave packets after they pass through the coupling region. Instead, due to the infinitely long lived coherence memory, SH effectively represents the superposition of two bifurcating wave packets instead of two independent packets.[11]

Though quite accurate for the description of adiabatic populations,[12] surface hopping does not generally give accurate diabatic populations, so the results of such approximate schemes are dependent on the representation employed. Moreover, surface hopping methods generally suffer from the "frustrated hop" problem where the classical subsystem kinetic energy is insufficient to make a hop between quantum subsystem states. This is actually a tunneling process that is classically forbidden.[6,13] Many hybrid methods have been proposed that try to combine the advantages of surface hopping and Ehrenfest mean-field like approaches, for example, the use of a smooth switching between the two types of forces in different regions,[14] Ehrenfest dynamics guided surface hopping[15] or the surface hopping dynamics with Ehrenfest excited state potential[16] approaches are two recent versions of such ideas.

Though many schemes for implementing mixed quantum-classical dynamics have been developed,[1] fundamental questions arise about the accuracy of dynamics methods that treat electronic and nuclear DOF on different dynamical footing.[17] Perhaps the most significant of these questions concerns if such approximate treatments can reliably capture the energy transfer processes between the two subsystems so as to reproduce detailed balance and yield the correct long time thermal equilibrium energy distribution between the systems.[18] To overcome this difficulty, the mapping Hamiltonian idea that exactly maps discrete quantum states onto continuous coordinates, was proposed by Miller and co-workers[19] here and elsewhere and enables consistent treatment for all DOF, at the classical, semi-classical, and full quantum dynamical levels. This idea replaces the evolution of the electronic subsystem by the dynamics of a system of fictitious mapping harmonic oscillators. With this approach, for example, the quantum amplitude transfer operator transforms as $|\beta\rangle\langle\lambda| \to \hat{a}_\beta^\dagger \hat{a}_\lambda$, where $\hat{a}_\lambda = \frac{1}{\sqrt{2\hbar}}(\hat{q}_\lambda - i\,\hat{p}_\lambda)$. For a given total Hamiltonian, $\hat{H} = \frac{\hat{P}^2}{2M} + \hat{h}_{el}$, the electronic Hamiltonian in the diabatic representation, $\hat{h}_{el} = \sum_{\beta,\lambda} |\beta\rangle\langle\beta|\hat{h}_{el}(\hat{R})|\lambda\rangle\langle\lambda|$, can be rewritten as

$$\hat{h}_{map}(\hat{R}) = \frac{1}{2\hbar}\sum_\beta h_{\beta,\beta}(\hat{R})\left(\hat{q}_\beta^2 + \hat{p}_\beta^2 - \hbar\right) + \frac{1}{2\hbar}\sum_{\lambda\neq\beta} h_{\beta\lambda}(\hat{R})(\hat{q}_\beta\hat{q}_\lambda + \hat{p}_\beta\hat{p}_\lambda), \quad (1)$$

where $(\hat{P}, \hat{R})$ and $(\hat{p}, \hat{q})$ represent the nuclear, and mapping oscillator phase space DOF, respectively.

In this paper, we show how to recover two different regimes: the mean-field – Ehrenfest, and state dependent force – surface hopping approaches, from a consistent theoretical framework that involves partially linearizing a path integral description of the full system dynamics with the mapping representation of the electronic DOF. The basic approach for linearizing within the mapping Hamiltonian formulation in order to derive procedures for mixed quantum-classical non-adiabatic dynamics that we extend here was originally developed by Shi and Geva.[20] With the approach outlined here we develop different procedures for partially linearizing the propagator in the nuclear DOF. By linearizing different parts of the phase of the integrand of the path integral density matrix propagator in the difference between the forward and backward paths of the nuclear DOF, either for the full phase angle as in Ref. 21 or linearizing the component of the phase arising from the equations of motion for the nuclear degrees of freedom,[22,23] we show that the force acting on the classical DOF can be, respectively, state dependent[21,24] such as the situation in surface hopping, or a mean-field like force[22,23] as with Ehrenfest dynamics.

Also, by employing an iterative scheme[24] that uses the linearized propagator as a short time approximation for a sequence of propagation segments, together with "focused" quantum subsystem initial condition sampling (a steepest descent integration approximation),[25] and a Monte Carlo switching algorithm that moves trajectories between representing coherence and population elements in the density matrix, the propagation can incorporate a version of "hopping" without *ad hoc* assumptions. Moreover, the theory can be derived in both a diabatic, and the adiabatic representation,[26] the latter having a more direct connection for comparison with surface hopping and other methods that use surface hopping ideas such as schemes based on the mixed quantum-classical Liouville (MQCL) equation.[27]

To explore the effectiveness of the different linearized approximate propagators and their iterative implementation as short time approximations, in Sec. III we first study how the different methods perform in reproducing exact results for nuclear subsystem quantities. In particular, we explore the ability of these different approaches to recover the bifurcation of the momentum distribution as the model systems studied pass through different arrangements of non-adiabatic coupling regions. Next, we explore the reliability of the different methods for reproducing the non-adiabatic electronic relaxation, focusing on electronic subsystem quantities. In the Appendix we demonstrate how the linearized short time propagators can be formulated in different representations and in the body of the paper we explore the effects of using approximate propagators on invariance of results to transformation between representations. The benchmark test problems we consider include: simple single avoided crossing scattering models and a dual avoided crossing Stueckelberg scattering problem,[1,5,7,8] as well as multi-state models of molecular photodissociation.[23,24,28] The Subsection III D explores the application of the linearized and iterative schemes to study relaxation in the spin-boson model of dissipative condensed phase non-adiabatic dynamics where we study the effects of temperature and the progression from short time non-equilibrium coherent dynamics to long time thermal equilibration.

II. THEORY AND METHODS

Direct implementation of the original mapping Hamiltonian by stationary phase approximation and classical trajectories encounters a fatal problem when $q_\beta^2 + p_\beta^2 < \hbar$, since, according to Eq. (1), some of the classical DOF can evolve on an inverted potential surface, proportional to $-h_{\beta,\beta}(R)$.[28–30]

Moreover, the population, $\rho_{\beta\beta} = \hat{a}_\beta^\dagger \hat{a}_\beta = \frac{1}{2\hbar}(\hat{q}_\beta^2 + \hat{p}_\beta^2 - \hbar)$, is not guaranteed to have a positive expected value when the approach is implemented approximately, e.g., with the LSC-IVR applied to multi-state systems.[28,31] This is due to the unphysical flow of zero point energy from the mapping harmonic oscillators in the classical limit[2,32] with the LSC-IVR approach that linearizes in the difference between forward and backward paths for *both* the mapping and nuclear DOF.

To overcome all these problems we use the coherent state representation of the mapping DOF[21,25] and linearize only in the nuclear DOF; allowing different mapping variable paths for the forward and backward propagators, i.e., partial linearization.

The quantity of interest is the evolution of the density matrix involving forward and backward propagation,

$$\begin{aligned}\langle R_t, n_t|\hat{\rho}|R_t', n_t'\rangle &= \sum_{n_0,n_0'}\int dR_0 dR_0' \langle R_t, n_t|e^{-\frac{i}{\hbar}\hat{H}t}|R_0, n_0\rangle \\ &\times \langle R_0, n_0|\hat{\rho}(0)|R_0', n_0'\rangle\langle R_0', n_0'|e^{\frac{i}{\hbar}\hat{H}t}|R_t', n_t'\rangle, \end{aligned} \quad (2)$$

here the total Hamiltonian is $\hat{H} = \hat{P}^2/2M + h_{map}(\hat{R}, \hat{p}, \hat{q})$, and n_t labels the basis states at time t. The propagator matrix elements in discrete path integral form are

$$\begin{aligned}\langle R_N, n_t|e^{-\frac{i}{\hbar}\hat{H}t}|R_0, n_0\rangle &= \int \prod_{k=1}^{N-1} dR_k \frac{dP_k}{2\pi\hbar}\frac{dP_N}{2\pi\hbar} e^{\frac{i}{\hbar}S_0} \\ &\times T_{[n_t,n_0]}[\{R_k\}], \end{aligned} \quad (3)$$

where the nuclear kinetic action is $S_0 = \epsilon\sum_{k=1}^{N}[P_k\frac{(R_k - R_{k-1})}{\epsilon} - \frac{P_k^2}{2M}]$, $T_{[n_t,n_0]}[\{R_k\}] = \langle n_t|e^{-\frac{i}{\hbar}\epsilon\hat{h}_{map}(R_{N-1})}\ldots e^{-\frac{i}{\hbar}\epsilon\hat{h}_{map}(R_0)}|n_0\rangle$, is the nuclear path dependent quantum transition amplitude and ϵ is the time step.

Using the coherent state representation with coherent state width parameter, $\gamma = 1/2$ (the choice of the width parameter will not influence the final results but may effect the numerical convergence[25]) and setting units so that $\hbar = 1$, the transition amplitude can be expressed as[21,25]

$$\begin{aligned}T_{[n_t,n_0]} &= \int dq_0 dp_0 \frac{1}{4}(q_{n_t} + ip_{n_t})(q_{n_0} - ip_{n_0}) c_t e^{iS_1(t)} \\ &\times e^{-\frac{i}{2}\sum_\beta(q_{\beta t}p_{\beta t} - q_{\beta 0}p_{\beta 0})} e^{-\frac{1}{2}\sum_\beta\left(q_{\beta 0}^2 + p_{\beta 0}^2\right)}, \end{aligned} \quad (4)$$

where $c_t = e^{-\frac{i}{2\hbar}\int_0^t d\tau\sum_\beta \hat{h}_{\beta\beta}(R)}$, $S_1(t) = \int_0^t L_1(\tau)d\tau$, with $L_1 = L_1^{cl} + \frac{1}{2}\sum_\beta h_{\beta\beta}(R)$, $L_1^{cl} = \sum_\beta p_\beta\dot{q}_\beta - h_{map}^{cl}(R)$ and

$$\begin{aligned}h_{map}^{cl}(R, p, q) &= \frac{1}{2}\sum_\beta h_{\beta\beta}(R)\left(p_\beta^2 + q_\beta^2\right) \\ &+ \frac{1}{2}\sum_{\lambda\neq\beta} h_{\lambda\beta}(R)(p_\lambda p_\beta + q_\lambda q_\beta). \end{aligned} \quad (5)$$

The term $\frac{\hbar}{2}\sum_\beta h_{\beta\beta}(R)$ in the action, S_1, that gives rise to the problem of inverting the potential can be eliminated as this term is cancelled exactly by the pre-factor, c_t[21,25] leaving $S_1^{cl}(t) = \int_0^t L_1^{cl}(\tau)d\tau$ in the phase. The combined forward and backward propagators in Eq. (2) can lead to phase cancellation that can cause problems for numerical implementation. Approximate schemes such as forward backward (FB) SC-IVR[10] can alleviate these difficulties. Alternatively, here we use the idea of partial linearization[33] in the nuclear DOF that involves transforming the forward and backward nuclear path variables, R and R', to mean and difference variables: $\bar{R} = (R + R')/2$ and $Z = (R - R')$, respectively, (with similar definitions for the mean and difference nuclear momenta, $\bar{P}$ and Y, respectively). The nuclear kinetic action difference becomes: $(S_0 - S_0') = \bar{P}_N Z_N - \bar{P}_1 Z_0 - \sum_{k=1}^{N-1}(\bar{P}_{k+1} - \bar{P}_k)Z_k - \sum_{k=1}^{N}[\frac{\epsilon}{m}\bar{P}_k - (\bar{R}_k - \bar{R}_{k-1})]Y_k$. The central approximation with the approaches we derive below involves truncating the phase difference in the combined transition amplitude terms to linear order in Z, based on the assumption that for short times, forward and backward nuclear paths will remain close to each other. This may appear to be a restrictive approximation that will only be valid for very short times for high dimensional problems but such linearization approximations have been shown to be reliable even when forward and backward paths differ significantly in some degrees of freedom.[34]

The Subsections II A and II B below, use the common starting point derived above to obtain two different short time approximate propagator schemes: an "Ehrenfest"-like dynamics approach with a mean force; and a "surface hopping" like algorithm, with a quantum subsystem state dependent nuclear force. In Sec. II C we present a general approach with which either of these two methods may be implemented iteratively to accurately extend these short time approximations to longer times.

The approaches developed in this section are derived using a diabatic representation of the discrete quantum system. The Appendix outlines the derivation of the adiabatic representation of the approach and in Sec. III we demonstrate that the results obtained from these types of calculations are independent of representation.

A. Mean-field, Ehrenfest-like theory: partial linearized density matrix (PLDM) propagation by linearizing the classical mapping Hamiltonian in the forward-backward path difference

With the linearization approximation, the key term is the classical mapping Hamiltonian difference $\Delta h_{map}^{cl} = [h_{map}^{cl}(R, p, q) - h_{map}^{cl}(R', p', q')]$ which can be written as

$$\begin{aligned}\Delta h_{map}^{cl} &= \left[h_{map}^{cl}(\bar{R}, p, q) - h_{map}^{cl}(\bar{R}, p', q')\right] + \mathcal{O}(Z^2) \\ &+ \frac{1}{2}\left(\nabla_{\bar{R}} h_{map}^{cl}(\bar{R}, p, q) + \nabla_{\bar{R}} h_{map}^{cl}(\bar{R}, p', q')\right) Z. \end{aligned} \quad (6)$$

Using this to expand the phase difference obtained by combining the forward and backward propagator terms in

Eq. (2) in terms of path difference, Z, and implementing the linearized approximation by propagating p and q with $h^{cl}_{map}(\bar{R}, p, q)$ (instead of $h^{cl}_{map}(R, p, q)$ or $h^{cl}_{map}(R', p', q')$), we obtain the following relationship connecting the various mapping variable dynamical quantities: $\sum_\beta p_\beta \dot{q}_\beta - h^{cl}_{map}(\bar{R}, p, q) = \frac{1}{2}\frac{d}{d\tau}(\sum_\beta p_\beta q_\beta)$, and the transition amplitude component of the phase difference becomes, $\Delta S^{cl}_1 = (S^{cl}_1[R(t), q(t), p(t)] - S^{cl}_1[R'(t), q'(t), p'(t)])$, which can be expanded as

$$\Delta S^{cl}_1 = \int_0^t \left[\frac{1}{2}\frac{d}{d\tau}\sum_\beta (p_{\beta\tau}q_{\beta\tau} - p'_{\beta\tau}q'_{\beta\tau}) + \mathcal{O}(Z^2_\tau) + \frac{1}{2}\nabla_{\bar{R}}\left(h^{cl}_{map}(\bar{R}_\tau, p_\tau, q_\tau) + h^{cl}_{map}(\bar{R}_\tau, p'_\tau, q'_\tau)\right) Z_\tau \right] d\tau. \tag{7}$$

With this result the first term in Eq. (7) cancels the boundary terms in $T_{[n_t,n_0]}$ given in Eq. (4) and similarly for the backward path transition amplitude, $T'_{[n'_0,n'_t]}$.

Combining forward and backward phase factors $(e^{i/\hbar(S_0 - S'_0)}T_{[n_t,n_0]}T'_{[n'_0,n'_t]})$ and performing the integrals over $Z_0 \ldots Z_{N-1}$, gives our approximation for $\rho_{n_t,n'_t}(R, R', t) = \langle \bar{R}_N + \frac{Z_N}{2}, n_t|\hat{\rho}(t)|\bar{R}_N - \frac{Z_N}{2}, n'_t\rangle$ with this scheme as

$$\begin{aligned}\rho_{n_t,n'_t}(R, R', t) = \sum_{n_0,n'_0}\int & d\bar{R}_0 dq_0 dp_0 dq'_0 dp'_0 G_0 G'_0 \\ & \times \frac{1}{4}(q_{n_0} - ip_{n_0})(q'_{n'_0} + ip'_{n'_0}) \\ & \times \int \prod_{k=1}^{N-1} d\bar{R}_k \frac{d\bar{P}_k}{2\pi\hbar}\frac{d\bar{P}_N}{2\pi\hbar}(\hat{\rho})^{n_0,n'_0}_W(\bar{R}_0, \bar{P}_1) \\ & \times \frac{1}{4}(q_{n_t} + ip_{n_t})(q'_{n'_t} - ip'_{n'_t})e^{\frac{i}{\hbar}\bar{P}_N Z_N} \\ & \times \prod_{k=1}^{N-1}\delta\left(\frac{\bar{P}_{k+1} - \bar{P}_k}{\epsilon} - F_k\right) \\ & \times \prod_{k=1}^{N}\delta\left(\frac{\bar{P}_k}{M} - \frac{\bar{R}_k - \bar{R}_{k-1}}{\epsilon}\right).\end{aligned} \tag{8}$$

Here, $G_0 = e^{-\frac{1}{2}\sum_\beta(q^2_{\beta 0} + p^2_{\beta 0})}$ and $G'_0 = e^{-\frac{1}{2}\sum_{\beta'}(q'^2_{\beta' 0} + p'^2_{\beta' 0})}$ are the initial distributions for the forward and backward mapping variables that satisfy $\dot{q}_{n_t} = \partial h^{cl}_{map}(\bar{R}_t)/\partial p_{n_t}$ and $\dot{p}_{n_t} = -\partial h^{cl}_{map}(\bar{R}_t)/\partial q_{n_t}$, and the nuclear trajectories are determined by a "mean-field" like force resulting from the different forward and backward mapping paths,

$$F_k = -\frac{1}{2}\nabla_{\bar{R}_k}\left[h^{cl}_{map}(\bar{R}_k, p_k, q_k) + h^{cl}_{map}(\bar{R}_k, p'_k, q'_k)\right]. \tag{9}$$

The mean nuclear DOF initial distribution is the partial Wigner transform: $(\hat{\rho})^{n_0,n'_0}_W(\bar{R}_0, \bar{P}_1) = \int dZ_0 \langle \bar{R}_0 + \frac{Z_0}{2}, n_0|\hat{\rho}|\bar{R}_0 - \frac{Z_0}{2}, n'_0\rangle e^{-\frac{i}{\hbar}\bar{P}_1 Z_0}$. We use factorized initial conditions, $\rho_0 = \rho^{eq}_{bath}(R)\rho_{sys}$, though the non-separable case can be treated.[35]

Numerical implementation of Eq. (8) involves sampling initial nuclear DOF from $(\hat{\rho})^{n_0,n'_0}_W(\bar{R}_0, \bar{P}_1)$, and mapping variables from the gaussian functions. However, with "focused" mapping variable initial conditions[25,36] that estimate the mapping variable initial condition integrals using a steepest descent approximation, the numerical convergence can be improved and typically only requires a small number ($\sim 10^4$) of trajectories to achieve convergence for standard model test problems. The accuracy of the focussed initial condition sampling will be discussed in detail later in Sec. III D. The product of δ-functions in Eq. (8) gives a time-stepping prescription for evolving the mean nuclear DOF with the force in Eq. (9). Finally quantum expectation values are computed using Eq. (8) and the state projected Wigner distribution,

$$(\hat{\rho})^{n_t,n'_t}_W = \int dZ_N e^{-\frac{i}{\hbar}\bar{P}_t Z_N}\left\langle \bar{R}_N + \frac{Z_N}{2}, n_t\middle|\hat{\rho}\middle|\bar{R}_N - \frac{Z_N}{2}, n'_t\right\rangle. \tag{10}$$

We refer to the approach presented above as PLDM propagation.[22]

The PLDM propagation scheme is a "mean trajectory" approach, but according to Eq. (9) it is different from "Ehrenfest" or LSC-IVR dynamics where the classical DOF force depends only on one set of mapping variables as $F^{Eh} = -\nabla_R h_{map} = -\sum_\beta \frac{1}{2\hbar}[(q^2_\beta + p^2_\beta - \hbar)\nabla_R h_{\beta,\beta} + \sum_{\lambda\neq\beta}(q_\beta q_\lambda + p_\beta p_\lambda)\nabla_R h_{\beta,\lambda}]$[10,37] rather than both the forward and backward propagating mapping variables with the partial linearized approach as in Eq. (9).

B. A surface hopping-like approach with state dependent force obtained by linearizing the integrand phase factor in the density matrix propagation

By following a different sequence of canceling and linearizing in the phase difference, a SH-like version of the theory can be derived known as iterative linearized density matrix (ILDM) propagation. It has been tested on various quantum dynamical problems.[24,38] While ILDM uses a surface hopping-like linearized expression as a short time approximation that is iterated to treat longer times, its convergence with large numbers of iterations can be problematic. The earlier linearized approach to non-adiabatic dynamics in the mapping formulation, or LANDmap[21,25] uses this same linearized approximation but without iteration. The statistical convergence of the LANDmap approach is superior to the iterated version but the linearized propagator underlying these methods is generally only reliable for short times and a balance between many iterations and statistical convergence must be considered. The mean trajectory linearized approximation underlying the PLDM scheme developed above, however, is generally accurate for much longer times for several classes of problems as demonstrated in the example applications presented below. The PLDM approach thus offers a significant improvement in statistical convergence while preserving high accuracy, even at long times for these classes of problems.

In this section, we briefly describe LANDmap[21] and its iterative version, ILDM,[24,39] based on a different type of linearization approximation. Up to Eq. (5), the development

of LANDmap and the PLDM approach are identical. Instead of directly applying the linearized approximation to the classical Hamiltonian as in the development of PLDM propagation, with LANDmap we first use the boundary term cancellation relation for the classical mapping Hamiltonian,

$$L_1^{cl} = \sum_\beta p_\beta \dot{q}_\beta - h_{map}^{cl}(R) = \frac{1}{2}\frac{d}{d\tau}\left(\sum_\beta p_\beta q_\beta\right). \quad (11)$$

Note this relation is exact, and there are different expressions of this form for the forward and backward nuclear paths, $R(t)$ and $R'(t)$. The major difference between LANDmap and the development of the PLDM propagation scheme outlined above is that here, we do not make the assumption that both p_β, q_β and $p'_{\beta'}$, $q'_{\beta'}$ propagate according to the classical mapping Hamiltonian evaluated along the same mean path, i.e., $h_{map}^{cl}(\bar{R})$. Rather, for the formal development of this theory the LANDmap short time approximation is used in which the forward and backward sets of mapping variables still propagate according to $h_{map}^{cl}(R)$ and $h_{map}^{cl}(R')$, respectively. Again we use the cancellation between the action phase $e^{\frac{i}{\hbar}S_1^{cl}(R,t)} = e^{\frac{i}{\hbar}\int_0^t L_1^{cl}(\tau)d\tau}$ $= e^{\frac{i}{2\hbar}\int_0^t \frac{d}{d\tau}(\sum_\beta p_\beta q_\beta)d\tau} = e^{\frac{i}{2\hbar}\sum_\beta (p_{\beta t}q_{\beta t} - p_{\beta 0}q_{\beta 0})}$ and the boundary terms in Eq. (4). Note that with the approximation underlying PLDM the action phase cancels the boundary condition term only to zero order, while in LANDmap/ILDM the total action phase cancels the boundary terms exactly. Now the propagators in Eq. (4) can be expressed as (with $\hbar$=1),

$$T_{[n_t,n_0]} = \int dq_0 dp_0 \frac{1}{4}(q_{n_t} + ip_{n_t})(q_{n_0} - ip_{n_0}) \times e^{-\frac{1}{2}\sum_\beta \left(q_{\beta 0}^2 + p_{\beta 0}^2\right)} \quad (12)$$

with a similar result for backward propagator. We proceed from this point and make the linearization approximation just as with the development of PLDM. Thus, we linearize the R and R' dependence of $p_\beta(R)$, $q_\beta(R)$ and $p_{\beta'}(R')$, $q_{\beta'}(R')$ in the difference between these forward and backward paths. This results in a phase factor in the integrand of the form $e^{i\times factor\times Z}$, and performing the integrals over dZ will, as above, make these phase factors in the path integral into δ-functions. Based on these considerations, we introduce the polar representation of the mapping variables in a similar fashion to the action angle variables employed by Meyer and Miller,[40]

$$r_{t,n_t}(\{R_k\}) = \sqrt{q_{t,n_t}^2(\{R_k\}) + p_{t,n_t}^2(\{R_k\})}$$
$$\Theta_{t,n_t}(\{R_k\}) = \tan^{-1}\left(\frac{p_{t,n_t}(\{R_k\})}{q_{t,n_t}(\{R_k\})}\right). \quad (13)$$

A more explicit form of Eq. (13) can be obtained if we use Hamilton's equation of motion for $p_{\tau n_t}$ and $q_{\tau n_t}$ derived from $\hat{h}_m^{cl}(R)$. The exact result is

$$\Theta_{t,n_t}(\{R_k\}) = \tan^{-1}\left(\frac{p_{0,n_t}}{q_{0,n_t}}\right) + \int_0^t d\tau \theta_{\tau,n_t}, \quad (14)$$

where

$$\theta_{\tau,n_t} = h_{n_t,n_t}(R_\tau) + \sum_{\lambda\neq n_t} h_{n_t,\lambda}(R_\tau)\frac{(p_{\tau n_t}p_{\tau\lambda} + q_{\tau n_t}q_{\tau\lambda})}{(p_{\tau n_t}^2 + q_{\tau n_t}^2)}. \quad (15)$$

With the LANDmap based approaches we now linearize in the difference between R and R' inside the phase factors for the forward and backward phases $\Theta_{t,n_t}(\{R_k\})$ and $\Theta'_{t,n'_t}(\{R'_k\})$, respectively.

There are two additional implicit approximations underlying the implementation of the LANDmap based propagation scheme.[21] The first involves assuming that the pre-exponential magnitude factors $r_{t,n_t}(\{R_k\})$ and $r'_{t,n'_t}(\{R'_k\})$ vary slowly with nuclear path compared to the exponential phase factor so that these different magnitude factors can be approximated by the magnitude evaluated along the mean path, $r_{t,n_t}(\{\bar{R}_k\})$, i.e., keeping terms only to zero order in the path difference in this slow varying part of the integrand. The exponential factor in the integrand, by contrast varies much more rapidly with path difference so the phase is kept to linear order in Z giving rise to the δ-functions in the approximate path integral kernel.

The second implicit approximation at the heart of the implementation of the LANDmap propagation is that, from this point of the development on, the time evolution of $p_{\tau n_t}$, $q_{\tau n_t}$ and $p'_{\tau n'_t}$ and $q'_{\tau n'_t}$ are governed by Hamiltonian $\hat{h}_{map}^{cl}(\bar{R})$, not $\hat{h}_{map}^{cl}(R)$ and $\hat{h}_{map}^{cl}(R')$, respectively, as we have now made the linearization approximation. One should notice that in the PLDM approach derived earlier, we also make similar approximations, but before the linearization approximation in the difference between R and R' has been made.

Combining the approximate expressions for the integrand developed so far, and integrating over Z, the final expression for the density matrix elements is obtained and it has the same form as Eq. (8), except now the force is state dependent since we have linearized each state dependent angle variable in Z. The LANDmap state dependent force thus has the form,

$$F_k^{n_t,n'_t} = -\frac{1}{2}\{\nabla_{\bar{R}_k} h_{n_t,n_t}(\bar{R}_k) + \nabla_{\bar{R}_k} h_{n'_t,n'_t}(\bar{R}_k)\} - \frac{1}{2}\sum_{\lambda\neq n_t} \nabla_{\bar{R}_k} h_{n_t,\lambda}(\bar{R}_k)\left\{\frac{(p_{n_t k}p_{\lambda k} + q_{n_t k}q_{\lambda k})}{(p_{n_t k}^2 + q_{n_t k}^2)}\right\} - \frac{1}{2}\sum_{\lambda\neq n'_t} \nabla_{\bar{R}_k} h_{n'_t,\lambda}(\bar{R}_k)\left\{\frac{(p'_{n'_t k}p'_{\lambda k} + q'_{n'_t k}q'_{\lambda k})}{(p'^2_{n'_t k} + q'^2_{n'_t k})}\right\}. \quad (16)$$

We note that this force cannot be generate from the original, or classical mapping Hamiltonian, so the mapping variables and nuclear trajectory are not governed by a single Hamiltonian[21] with in this LANDmap approach. This is quite different from the PLDM approach developed earlier in this paper, or other semi-classical approaches where the force is generated from the mapping Hamiltonian.[41–44] This is also different from the Pechukas semi-classical approach to non-adiabatic dynamics, where the transition amplitude and trajectory must be determined by self-consistent iteration.[4]

The algorithm developed in this section is the so called LANDmap[21] approach and it has been used as a short time segment propagator that can be extend to longer times by iteratively including multiple time slices giving the ILDM propagation method.[24] Between the short segments, Monte Carlo sampling is used to choose the specific pair of state labels that give the most important contribution to the long time path

integral. These new selected states are then used to initialize the next propagation segment giving the ILDM algorithm its surface hopping flavor. Unlike surface hopping approaches, however, the ILDM approach samples not only population terms as with regular SH methods, but the ILDM trajectories also spend time representing nuclear evolution of the coherence density matrix elements. The basic iterative scheme is outlined below.

C. Iterative implementation for long time propagation

Linearized approximations, such as both those derived above, are generally only accurate for short times. One way to overcome this limitation is to apply the linearized approximation iteratively[24] for a series of segments or short time slices obtained by inserting resolutions of the identity into the exact, full time interval, density matrix propagator. The result, for example, of concatenating two segments using the PLDM propagator of the form in Eq. (8) as the short time approximation, can be evaluated by performing the integration over intermediate path difference variables by noticing that the boundary terms of the two segments can be computed as: $\int dZ_N e^{i\bar{P}_N Z_N} e^{-i\bar{P}_{N+1}Z_N} \sim \delta(\bar{P}_N - \bar{P}_{N+1})$. The final result for concatenating these two approximate linearized short time segments giving $\hat{\rho}(2t)$ is thus,[24]

$$
\begin{aligned}
&\left\langle \bar{R}_{2N} + \frac{Z_{2N}}{2} n_{2t} | \hat{\rho}(2t) | \bar{R}_{2N} - \frac{Z_{2N}}{2} n'_{2t} \right\rangle \\
&= \int \prod_{k=N+1}^{2N-1} d\bar{R}_k \frac{d\bar{P}_k}{2\pi\hbar} \frac{d\bar{P}_{2N}}{2\pi\hbar} e^{\frac{i}{\hbar}\bar{P}_{2N}Z_{2N}} \\
&\quad \times \delta\left(\frac{\bar{P}_{k+1} - \bar{P}_k}{\epsilon} - F_k \right) \prod_{k=N+1}^{2N} \delta\left(\frac{\bar{P}_k}{M} - \frac{\bar{R}_k - \bar{R}_{k-1}}{\epsilon} \right) \\
&\quad \times \sum_{n_t, n'_t} \int d\bar{R}_N \frac{d\bar{P}_N}{2\pi\hbar} dq_N dp_N dq'_N dp'_N G'_t G_t \delta(\bar{P}_N - \bar{P}_{N+1}) \\
&\quad \times \frac{1}{4}(q_{n_{2t}} + ip_{n_{2t}})(q_{n_t} - ip_{n_t}) \frac{1}{4}(q'_{n'_{2t}} - ip'_{n'_{2t}})(q'_{n'_t} + ip'_{n'_t}) \\
&\quad \times \delta\left(\frac{\bar{P}_N}{M} - \frac{\bar{R}_N - \bar{R}_{N-1}}{\epsilon} \right) \int \prod_{k=1}^{N-1} d\bar{R}_k \frac{d\bar{P}_k}{2\pi\hbar} \\
&\quad \times \delta\left(\frac{\bar{P}_{k+1} - \bar{P}_k}{\epsilon} - F_k \right) \prod_{k=1}^{N} \delta\left(\frac{\bar{P}_k}{M} - \frac{\bar{R}_k - \bar{R}_{k-1}}{\epsilon} \right) \\
&\quad \times \sum_{n_0, n'_0} \int d\bar{R}_0 dq_0 dp_0 dq'_0 dp'_0 G'_0 G_0 (\hat{\rho})_W^{n_0, n'_0}(\bar{R}_0, \bar{P}_1) \\
&\quad \times \frac{1}{4}(q_{n_t} + ip_{n_t})(q_{n_0} - ip_{n_0}) \frac{1}{4}(q'_{n'_t} - ip'_{n'_t})(q'_{n'_0} + ip'_{n'_0}).
\end{aligned}
\tag{17}
$$

We refer to the algorithm based on this expression as the iterative-PLDM (IPLDM) propagation approach. In a similar fashion, the ILDM approach is obtained by replacing the mean surface Ehrenfest-like force in this IPLDM expression by the state dependent LANDmap force in Eq. (16) and substituting the polar representations for the Cartesian mapping variable polynomials that weight each sampled path's contribution to the density matrix. A general approximate implementation of this type of trajectory based algorithm is detailed in Ref. 24 and can be summarize as follows: (1) Sum over forward and backward initial quantum states n_0, and n'_0, and select the final density matrix element of interest, n_t, and n'_t; (2) Sample mean environment path initial position $\bar{R}_0$, and momentum $\bar{P}_1$ from the Wigner distribution $[\hat{\rho}]_W^{n_0,n'_0}(\bar{R}_0, \bar{P}_1) = \int dZ_0 \langle \bar{R}_0 + \frac{Z_0}{2} n_0 | \hat{\rho} | \bar{R}_0 - \frac{Z_0}{2} n'_0 \rangle e^{-\frac{i}{\hbar}\bar{P}_1 Z_0}$;[21,35] (3) Propagate the environmental subsystem degrees of freedom using classical mechanics with the appropriate force for the given algorithm. At time t, the summation over n_t and n'_t for a particular trajectory is done by Monte Carlo importance sampling that involves randomly choosing the "occupied" density matrix element that defines the initial condition for the next time segment of density matrix propagation by re-focussing the initial state for propagation from t to 2t on one particular initial density matrix element. The focusing approximation is thus made to restart each new segment. This importance sampling approach tames the potential exponential divergence in number of trajectories with increasing number of time segments. The details of this algorithm can be found in Ref. 24 for the ILDM implementation.

Generally we find that the statistical convergence of these different trajectory based iterative schemes, IPLDM or ILDM, are similar, and require ensembles of typically 10^6–10^7 trajectories for a range of simple scattering to condense phase model problems.[24] In contrast, for the same types of models we find that the mean-field PLDM approach requires much smaller ensembles of only 10^3–10^4 trajectories to achieve the same level of statistical convergence, but its accuracy at longer times is limited.

We should again stress, however, that although the actual numbers of trajectories required to achieve convergence with these iterative schemes are similar, the IPLDM scheme is significantly more efficient since it evolves all the different density matrix elements using a single set of trajectories that are propagated using the same mean-field force that is independent of state labels. With the ILDM procedure, on the other hand, trajectories for each different density matrix element must be generated with different state dependent forces so on the order of n^2_{state} more auxiliary trajectories must be run with the ILDM calculation.

This iterative algorithm is similar to the trotter based Monte Carlo approach developed to implement the MQCL equation by Kapral and co-workers.[27] However, it should be noted that the importance sampling procedure with the MQCL scheme is based on the relative amplitude of the real part of Liouville operator in the adiabatic representation, while the iteration scheme used here employs the relative absolute value of density matrix elements in either the diabatic or adiabatic (see the Appendix) representations as the basis of the importance sampling approach.

Further, the delta function $\delta(\bar{P}_N - \bar{P}_{N+1})$ in Eq. (17), for the ILDM or IPLDM implementation requires conservation of nuclear momentum from one time slice to the next. This means that an individual trajectory does not conserve

the energy between iterations for these approaches. However, the ensemble of the trajectories should conserve the energy on average.[24] This is quite a different situation compared to the MQCL[27] or fewest switches surface hopping (FSSH),[1,5,6] approaches, where, by construction, individual trajectories conserve energy during the hopping process. In Sec. III we present results for a new approximate iterative linearized approach in which we experiment with a "jump" implementation that is based on similar energy conservation ideas to alleviate the problems arising from having to average oscillatory phase factors. The convergence of this new approximate approach, and the quality of the results it produces, as outlined in Sec. III, are extremely promising.

III. RESULTS

In this section, we present the results of model calculations using the different algorithms outlined in Sec. II with the goal of testing the reliability of these different approximate methods for reproducing the results of exact quantum calculations in various important contexts. We compare the relative merits of these different linearized approximations with those of other approximations including different types mixed quantum-classical and semi-classical methods that are formulated in terms of either surface hopping or mean-field like approaches.

First we explore the application of these methods to situations in which the linearized methods are able to reproduce the electronic state density matrix properties, but they fail to give reliable representations of nuclear phase space dependent properties such as nuclear position and momentum distributions. These nuclear quantities are often more sensitive[10,30] and capable of revealing the shortcomings of the different approximations thus enabling us to explore various approaches for overcoming these shortcomings. In particular, we use one-dimensional two state models and conditions in which, asymptotically, the two electronic states have significantly different energies so the nuclear momentum distribution shows two distinct peaks arising from non-adiabatic dynamics in the different electronic states.[10,30] Mean-field methods, by the single mean surface Ehrenfest nature of their underlying dynamics, cannot reproduce this type of bifurcated nuclear motion.[10,30] We show, however, that the iterative implementation of the linearized short time approximations outlined above can recover the basic physical phenomenon of bifurcation of the nuclear distributions in regions of non-adiabatic transitions, and moreover, these iterative procedures reliably capture the decoherence dynamics that results as the nuclear packets on the different coupled electronic surfaces diverge from one another.

Next we employ a simple one-dimensional, two state model, Tully's "Stueckleberg scattering" problem,[1] to demonstrate how the algorithms outlined here[22] can be implemented in different representations, for example, we show how adiabatic or diabatic implementations may be used equally well with in the approximations of these methods and different representations may gain numerical advantage depending on the nature of the problem at hand.

As mentioned above, the "focusing" approximation is an important component of the iterative implementation that makes the approach tractable. We demonstrate that this approximation does, however, affect the accuracy of the propagation. If the iteration, and it's use of the focusing approximation can be avoided, for example, if the PLDM approach can be applied at longer times and the full mapping variable initial condition distribution is sampled, rather than having to make successive steepest approximations to the mapping variable initial condition integrals at each iteration, the PLDM procedure is shown to give highly accurate results. If it is necessary to iterate the focusing approximation many times this can lead to inaccuracy in both electronic populations and nuclear distributions, the basic physics of bifurcating distributions, however, is qualitatively preserved with the iterative approaches implemented using focused initial conditions.

The iterated linearized short time approximate density matrix propagation approaches are generally computationally expensive since, as we demonstrate below, they recover the physics underlying the non-adiabatic bifurcating nuclear distributions by accumulating phase factors from different paths, thus capturing this phenomenon through interference effects. There is a long history of treating this type of behavior in an *ad hoc* fashion using energy conserving jumps between adiabatic electronic surfaces with in the surface hopping framework. The resulting algorithms, like Tully's fewest switches surface hopping approach, are highly numerically efficient and generally very accurate, albeit somewhat *ad hoc*. With the aim of improving algorithmic efficiency we incorporate a velocity rescaling approach, reminiscent of surface hopping algorithms, with in the iterative linearized scheme and demonstrate that the new hybrid approach can give very accurate results with significantly improved numerical efficiency.

In Subsection III B we compare the results of various approaches for more challenging multi-surface applications modeling non-adiabatic photodissociation dynamics,[24,25,28] and in Subsection III D we also study the usefulness of the different approaches for treating the spin-boson model of condensed phase non-adiabatic dynamics, to explore how these approximate algorithms are expected to perform in applications to model excited state chemical dynamics in complex solution phase environments.

A. Nuclear phase space distributions from linearized, and iterative linearized mapping Hamiltonian dynamics

To focus our investigation of the detailed performance of the different linearized density matrix propagation implementations we have first chosen the simple two state avoided crossing model of Tully (Tully 1).[1] The panels of Fig. 1 compare results obtained using various approximate schemes for computing the time evolution of diabatic state populations with exact results for different incident scattering energies or wave packet momenta. We generally find, both at high and low incident wave packet momentum, that all approaches considered here give good results for this electronic state population dynamics.

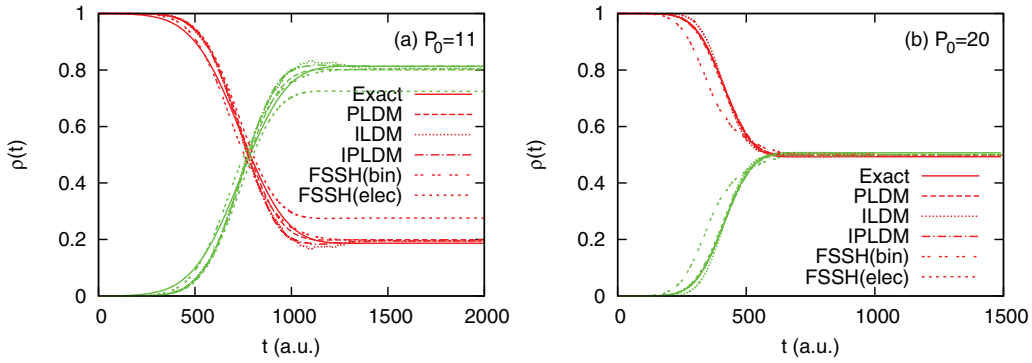

FIG. 1. Diabatic electronic population dynamics for the Tully 1 two state simple avoided crossing scattering model. Results for various linearized and iterative propagation algorithms are compared as detailed in the text. Left panel (a) corresponds to lower incident wave packet momentum situation and right panel (b) gives results for higher incident wave packet momentum.

The FSSH scheme, however, gives ambiguous diabatic state populations as this approach is formulated in a representation dependent, adiabatic fashion.[2,6] With FSSH, the dynamics is run in the adiabatic representation, and there are a variety of ways of computing the diabatic state populations, for example, counting or "binning" the number of trajectories in a given adiabatic state and then transforming to the diabatic representation (bin),[2,6] or transforming the adiabatic expansion coefficients directly to diabatic coefficients and then averaging the resulting diabatic electronic populations (elec).[2,6] The quality of these different FSSH approaches to computing diabatic state populations is seen to vary with the conditions studied, e.g., in Fig. 1 we see the different FSSH diabatic population estimators give different quality agreement depending on incident wave packet momentum.

The panels of Fig. 2 compare the results of various calculations of the nuclear momentum distribution for this model obtained using different implementations of the linearized approximate propagation methods. We see that, while the mean-field PLDM approach, for example, gives a very accurate description of the evolution of the electronic populations (Fig. 1), the PLDM momentum distribution results presented in Fig. 2 show that the approach fails to capture the bimodal nature of the exact nuclear momentum distribution that results from the asymptotic populations moving on the different electronic surfaces. Rather, the mean-field PLDM propagation scheme, gives a nuclear momentum distribution with a broad single peak resulting from an ensemble of trajectories whose nuclear motion occurs over a mean surface after passing through the non-adiabatic coupling region.

The other curves in the panels of Fig. 2 present the asymptotic nuclear momentum distributions obtained using the various linearized expressions outlined in Sec. II as short time approximations and iterating these to generate longer time propagation. Thus the curves labeled ILDM( ) and IPLDM( ) use the LANDmap (state dependent) and PLDM (mean-field) short time approximations, and the letters in the brackets refer to nuclear momentum distribution results obtained with: (P) accumulating the distributions using the full trajectory phase factor weights, i.e., the product of mapping variable polynomial factors, e.g., $\frac{1}{4}(q_{n_t}+ip_{n_t})(q_{n_0}-ip_{n_0})\frac{1}{4}(q'_{n'_t}-ip'_{n'_t})(q'_{n'_0}+ip'_{n'_0})$ in Eq. (17), (O) without trajectory phase weights (i.e., the distribution is accumulated with all trajectory weights set to unity), and finally (J) where we employ a new surface hopping-like algorithm that branches trajectories into different density matrix elements at the end of each time slice, but conserves energy during such "jumps" by rescaling the nuclear velocities. With this branching or "jump" approach the momentum distributions displayed in the figure are computed without including trajectory phase weights in the average. We outline the ideas underlying this new "jump" approach later in this section.

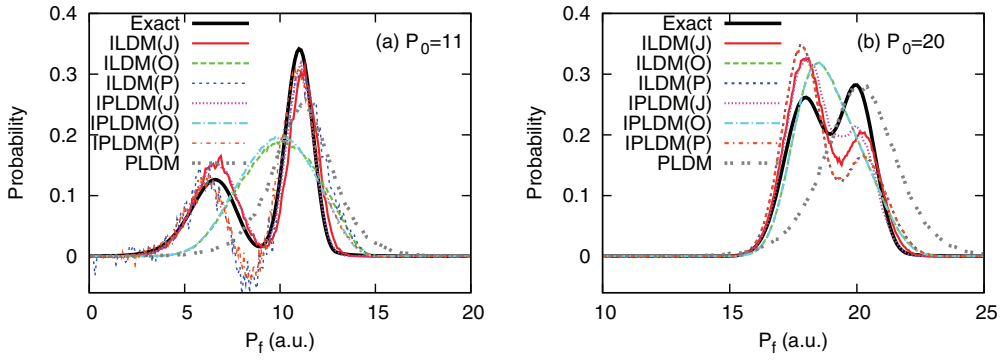

FIG. 2. Asymptotic nuclear momentum distributions for the Tully 1 two state simple avoided crossing scattering model. Results for various linearized and iterative propagation algorithms are compared as detailed in the text. Left panel (a) corresponds to lower incident wave packet momentum situation and right panel (b) gives results for higher incident wave packet momentum.

The results presented in the ILDM(P) and IPLDM(P) curves demonstrate that these fully iterated algorithms including all the trajectory weights and phases converge to reproduce the underlying physics of the bimodal asymptotic nuclear momentum distributions. These implementations, however, cannot give the exact results as they make the focused initial condition sampling approximation at the beginning of each time slice. We see that this approximation can result in incomplete phase cancellation in the accumulated average over the phase factor weighted trajectories and give regions where the calculated asymptotic nuclear momentum distributions are actually negative. This unphysical behavior is significantly less pronounced in the distributions calculated at higher incident wave packet momentum.

Comparing the ILDM(P) or IPLDM(P) results with those obtained leaving out the trajectory phase weights, i.e., ILDM(O) or IPLDM(O) makes it clear that interference effects play a critical role in generating the bimodal nuclear momentum distribution with these types of algorithms. For this model the ILDM(O) or IPLDM(O) momentum distributions have single broad, undifferentiated peak and the phase weights included in the ILDM(P) or IPLDM(P) calculations give destructive interference effects that produce the "dip" in the distribution giving the bimodal character, while constructive interference between phase weighted trajectories, for example, in the incident momentum $P_0 = 11$ example distribution, result in significant enhancement of the low momentum part of the distribution giving the final overall bimodal shape.

Here we emphasize that the IPLDM(P) results are obtained with an algorithm that actually uses a mean-field type of force, which is not a state dependent single surface force like that used to obtain the ILDM(P) results. These approaches give accurate momentum distributions purely as a result of interference and phase averaging effects, which is a similar mechanism to that underlying the SC-IVR theory, and its forward-backward implementation FB-IVR.[10]

The most significant problem facing the iterative implementation of these linearized short time approximate propagation schemes is the convergence of the fully phase weighted averages as described above. Typically ensemble sizes of at least 10^7 trajectories are required, for example, to represent the interference effects that lead to the bimodal momentum distribution in the results presented here. For comparison, results for the (O) methods that leave out the phases can be converged with fewer than 10^4 trajectories. Generally, despite similarly large ensemble sizes to achieve convergence of the phase factor averages, the IPLDM approach is a significantly more efficient calculation since to evolve for a time step requires only a single propagation where as the number of propagations required to evolve for a single step of the ILDM method is on the order of the square of the number of states. Also we generally find that the PLDM propagator is a superior short time approximation to the LANDmap propagator so IPLDM propagation requires fewer iterations than the ILDM approach to achieve similar accuracy.

The ILDM(J) and IPLDM(J) results displayed in the panels of Fig. 2 represent a first attempt at formulating a new approach that tries to overcome these convergence issues in averaging phase factors by using additional approximations. The iterative linearized "jump" methods that were used to generate the results presented as the ILDM(J) and IPLDM(J) momentum distributions in Fig. 2 are inspired by the ideas behind surface hopping-like algorithms and their successes. Essentially, the notion here is that when trajectories in our ensemble branch between representing different density matrix elements they pick up phases that are related to an "energy gap" such as quantity, and weights that normalize for our use of the absolute amplitude of the density matrix as a branching probability distribution between the different density matrix elements (see iterative scheme algorithmic details presented in Ref. 24). By choosing the starting nuclear momentum for the next time slice to be equal to the finishing nuclear momentum of the previous time slice plus a term proportional to the square root of the energy gap, such as quantity, the phase factors at the boundaries of successive time slices can give stationary phase-like conditions that are equivalent to conserving the effective energy during the jump. By absorbing the effects of the phase factors into an energy conserving adjustment to the nuclear dynamics, these phase factors no longer need to be included as weights in the average and the momentum distributions, for example, are determined by simply accumulating unit weighted histogram entries of the modified trajectory momenta. Note incorporating the phase factor weights in this way modifies the momentum conserving δ-function term in Eq. (17), the additional contributions to the phase shift the argument of the δ-function so that energy is conserved in passing from one propagation segment to the next.

To summarize these jump methods: at the end of the first propagation time slice that runs from 0 to t in N steps with starting density matrix labels n_0, n_0' and sampled final labels n_t, n_t' the terminal momentum is readjusted to determine the starting momentum of the new time slice as,

$$P_{N+1}^2 = P_N^2 + 2M(H_{n_0,n_0'}(\bar{R}_k) - H_{n_t,n_t'}(\bar{R}_k)). \tag{18}$$

For the ILDM(J) version the following energy term is employed:

$$\begin{aligned} H_{n_t,n_t'} = {} & \frac{1}{2}[h_{n_t,n_t}(\bar{R}_k) + h_{n_t',n_t'}(\bar{R}_k)] \\ & + \frac{1}{2}\sum_{\lambda\neq n_t} h_{n_t,\lambda}(\bar{R}_k)\left\{\frac{(p_{n_t}p_\lambda + q_{n_t}q_\lambda)}{(p_{n_t}^2 + q_{n_t}^2)}\right\} \\ & + \frac{1}{2}\sum_{\lambda\neq n_t'} h_{n_t',\lambda}(\bar{R}_k)\left\{\frac{(p_{n_t'}'p_\lambda' + q_{n_t'}'q_\lambda')}{(p_{n_t'}'^2 + q_{n_t'}'^2)}\right\}, \end{aligned} \tag{19}$$

while with the IPLDM(J) implementation the energy term takes the form,

$$H_{n_t,n_t'} = \frac{1}{2}\left[h_{map}^{cl}(\bar{R}_k, p_k, q_k) + h_{map}^{cl}(\bar{R}_k, p_k', q_k')\right]. \tag{20}$$

In multidimensional systems it is critical to make these nuclear momentum adjustments that conserve energy during jumps in the right direction, this can be accomplished with the different approximate short time propagators using the directions of the PLDM or LANDmap forces in Eqs. (9) and (16), respectively. The development of this momentum jump approach is currently being explored, and the preliminary results presented here are very promising.

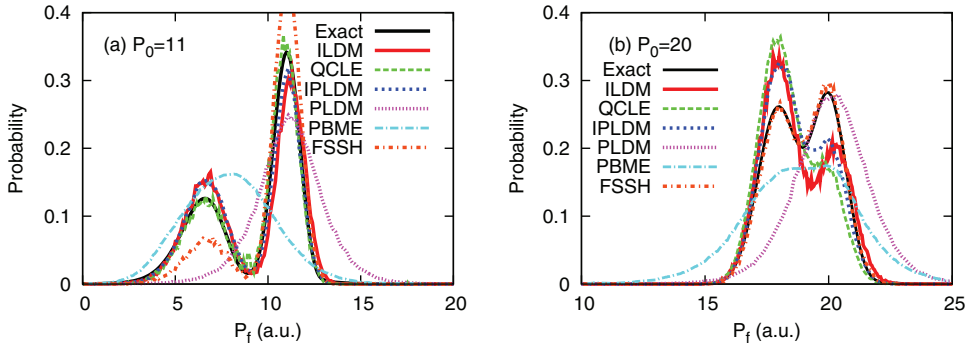

FIG. 3. Asymptotic nuclear momentum distributions for the Tully 1 two state simple avoided crossing scattering model. Results for various propagation algorithms are compared as detailed in the text. Left panel (a) corresponds to lower incident wave packet momentum situation and right panel (b) gives results for higher incident wave packet momentum.

The statistical convergence of this jump implementation of the iterative linearized propagation scheme is significantly superior to that of the full phase factor weighted algorithm. For example, the asymptotic momentum distributions labeled ILDM(J) and IPLDM(J) in Fig. 2 are converged with $\sim 10^4$ trajectories and are generally found to be in very good agreement with the exact results. To summarize, the different version of our theories presented here have common features with semi-classical theories such as FB-IVR (our IPLDM(P)) or mixed quantum-classical theories such as FSSH (our ILDM(J)).

Figure 3 compares the momentum distributions obtained from this jump implementation of the iterative linearized propagation schemes for this model with exact results and various other approximations including: the quantum-classical Liouville equation approach,[30] which can accurately represent the bifurcating distribution. Tully's FSSH algorithm that gives excellent results at high incident momentum but gives only a qualitative account of the relative magnitudes of the momentum distribution peaks, and the Poisson bracket master equation (PBME) approach,[30] which gives the incorrect physics of a single peaked momentum distribution typical of a mean-field approximate approach.

To demonstrate just how serious an error can be made in these sensitive nuclear distribution quantities using mean-field like approaches for some classes of problems, Miller and co-workers[10] explored a model in which there is a large mismatch in the asymptotic energy gap between states and a region of strong coupling on the wall where this large gap opens up. These model surfaces are presented in the lower panel of Fig. 4. The upper panel (a) compares exact benchmark results for the asymptotic momentum distributions for this model computed with results from various mean-field approaches including: Ehrenfest, the LSC-IVR and the focused and sampled versions of the PLDM propagation approach. For the selected incident momentum the mean-field potential surface experienced by LSC-IVR or PLDM trajectories has a barrier that can scatter trajectories in either forward or backward directions. When the full distribution of initial conditions is sampled we see that the mean-field approaches give completely unphysical asymptotic momentum

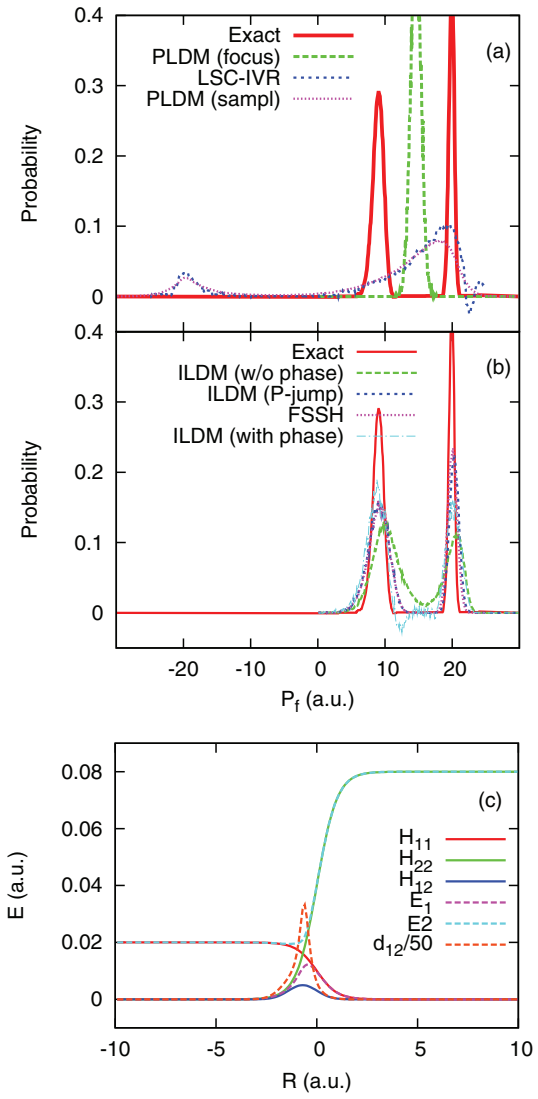

FIG. 4. Upper panels (a) and (b) show asymptotic nuclear momentum distributions computed with various algorithms for a gaussian wave packet incident from the left on the lower surface of the two state Hamiltonian model presented in the lower panel (c). Details of the calculations are the same as given in Ref. 10. Upper panel (a) shows results for various linearized approaches. Middle panel (b) compares results obtained using various iterative algorithms with fewest switches surface hopping results.

distributions with a positive momentum forward scattering peak and a negative momentum backward scattering peak in marked contrast to the exact results that show two peaks involving only forward scattering of trajectories on either of the two widely separated surfaces. Fortuitously, the focused initial condition sampling PLDM gives just forward scattering but only a single peak in the nuclear momentum distribution results from the mean-field dynamics. This occurs since the lower energy component initial conditions that cannot get over the barrier in the forward direction are removed when only a single point in the mapping variable initial condition distribution is sampled with the steepest descent approximation to the initial condition integrals underlying the focusing approach. The lower panel (b) of Fig. 4 shows clearly that the iterative implementation of the various linearized approaches outlined above gives a qualitatively reliable description of the dynamics of these challenging model conditions.

As a final note, in this subsection we have confirmed that for nuclear DOF, the distribution of coordinates[45] or momenta[10] produced by methods that employ mean-field Ehrenfest-like forces such as LSC-IVR can be qualitatively in error. As we will demonstrate in Subsection III B this can have profound problems for predicting electronic state relaxation dynamics with such approaches, though these problems are mitigated to a significant extend for some mean-field like methods such as the PLDM propagation approach. These well-known disadvantages of mean-field like methods can be addressed by surface hopping schemes[1,46] but many such approaches involve *ad hoc* steps in their implementation. The forward-backward IVR (FB-IVR) approach[10,45,47] provides a relatively inexpensive alternative that is derivable from first principles and can solve these problems in many situations. The iterative linearized short time approximate propagation methods outlined here are also based on well-defined approximations and overcome the problems associated with mean-field propagation and can be made very competitive in computational cost.

B. Multi-state electronic relaxation dynamics from linearized propagation methods

As noted earlier, the electronic relaxation dynamics is generally significantly less sensitive to approximations in the treatment of the full system quantum propagation than the nuclear distributions as explored in Subsection III A. However, there can be appreciable effects on electronic properties associated with these approximations and to explore these here, we use a three coupled Morse potential energy surface form that is capable of modeling different scenarios for multi-state non-adiabatic photodissociation dynamics.[23,24,28] The diabatic potentials and electronic couplings of the two different models we explore in this subsection are displayed in the bottom panels of Fig. 5. In each case the initial zero momentum gaussian wave packet is placed on diabatic state 1 centered at the position of vertical arrow, thus modeling a Franck-Condon initial molecular excitation. The parameters for the potentials and initial wave packets can be found in Ref. 28.

The upper panels (a) and (b) of Fig. 5 show how the iterative PLDM scheme (IPLDM results) gives an excellent description of non-adiabatic electronic relaxation for much longer times and through multiple avoided crossing regions, giving results that agree quantitatively with exact quantum, and ILDM propagation calculations. As outlined in Sec. II C, these iterative implementation algorithms require the focusing approximation to initiate each new time slice and as we have seen in the studies reported above this can result in inaccuracies in nuclear distributions that may also effect the reliability of electronic relaxation but for the models and range of parameters considered here, such effects are relatively insignificant.

The middle panels (c) and (d) of Fig. 5 compare exact benchmark electronic state populations with approximate results computed for these models using various linearized schemes including LSC-IVR and PLDM propagation. The PLDM results, which are obtained by linearizing in the difference between the forward and backward paths of only the nuclear degrees of freedom while keeping interference effects between the forward and backward mapping variable paths, give electronic relaxation dynamics that match very closely with exact results. The LSC-IVR scheme, on the other hand, which linearizes in the difference between forward and backward paths of all DOF, fails to capture even the qualitative trends in electronic state relaxation, and unfortunately gives unphysical negative populations.[28] The PLDM description of the electronic relaxation does start to degrade at longer times as the system passes through multiple regions of non-adiabatic coupling and the nuclear trajectories, with in the mean-field approximation at the heart of the PLDM approach, move on an averaged effective potential surface instead of actually branching onto the different component potential surfaces and experiencing different state dependent forces. Since the PLDM propagation scheme is accurate for much longer times, incorporating it in an iterative implementation offers an extremely efficient algorithm for reliably propagating to longer times as significantly fewer of these more accurate time slices are required.

C. Linearized mapping Hamiltonian dynamics in the diabatic and adiabatic representations

In this section we present the first results computed using the adiabatic representation of our linearized density matrix propagation scheme[26] that is outlined in the Appendix. The purpose of developing these algorithms in different representations is that, for physical reasons, some problems may be more efficiently treated in one representation than in another. For exact propagation methods, the representation adopted in which to evolve the system is irrelevant as we can trivially transform the results between representations. However, when approximations to the dynamics are employed, as is the case with our linearization schemes, or even when we iterate a linearized short time approximation and have to use focused initial conditions to start each time slice, there is no guarantee that the diabatic and adiabatic algorithms will produce results that can be identically transformed between one another.

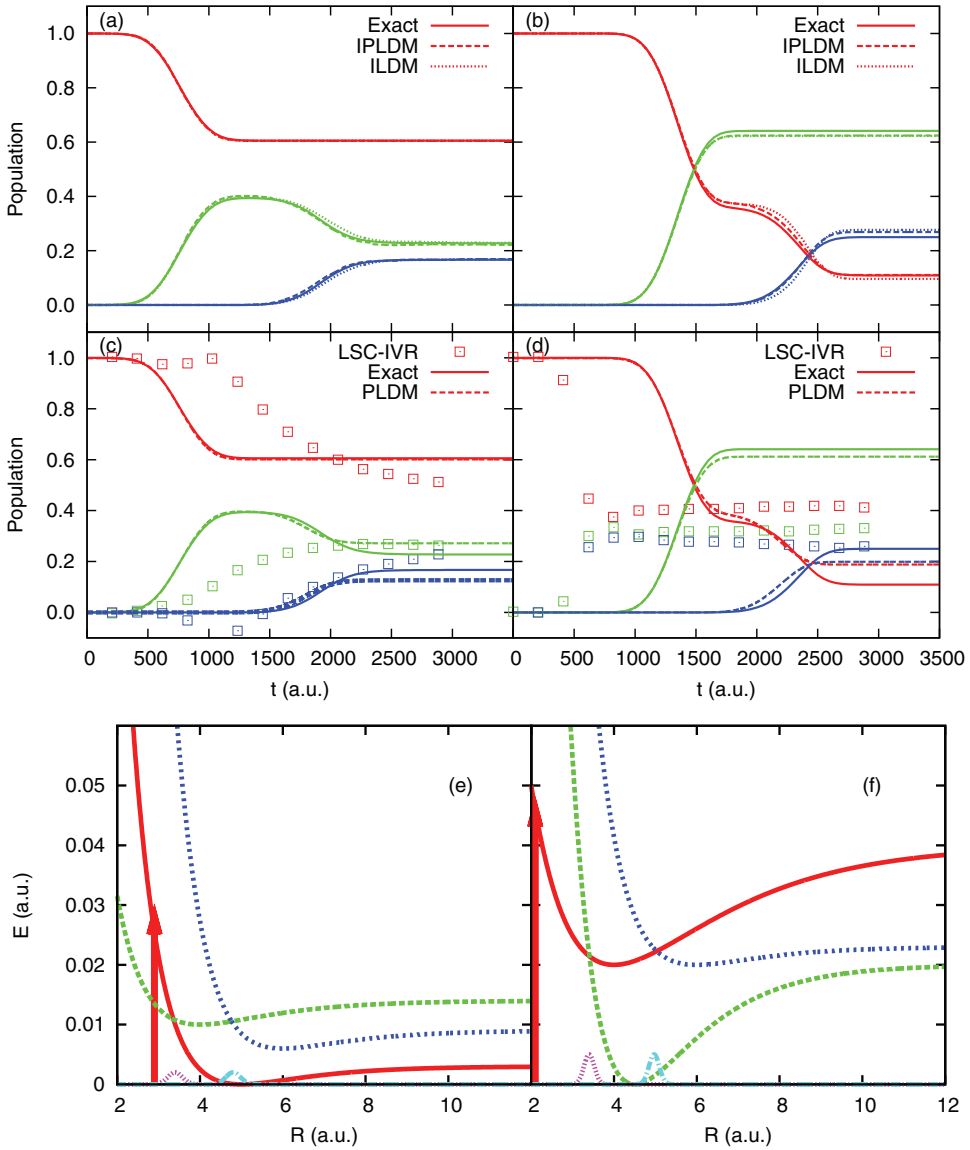

FIG. 5. Results of calculations exploring the accuracy of different linearized and iterative approaches for treating electronic relaxation for a multiple coupled Morse potential surface model of molecular photo-dissociation. Details of model parameters can be found in reference 28. Bottom panels show nuclear coordinate dependence of surfaces and couplings used in the model Hamiltonian. Arrows indicate initial positions of nuclear wave packets. Middle panel compares exact results for population dynamics with results obtained from various linearized approximate propagation methods. Upper panel shows the high quality results obtained by iterating the different linearized short time approximate propagators. The results presented here use 30 iterations.

As a concrete test problem we again use the two state, dual avoided crossing, Stueckelberg scattering model, Tully 2.[1] In Fig. 6 we compare exact benchmark results for the time dependence of the electronic state populations and coherences with those obtained using the various approximate algorithms. The left panel presents results in the diabatic representation, and the right in the adiabatic representation. The PLDM and ILDM algorithms are constructed so that the propagation takes place in the diabatic representation, where as the propagation of the AD-ILDM and FSSH methods is performed with adiabatic basis states. The generally excellent agreement between the results computed in different representations suggests that the approximations underlying these propagation methods preserve unitarity of the propagation in the different representations. We note that the diabatic algorithms and our adiabatic linearized approaches include the non-adiabatic wave function curvature terms ($G_{\lambda,\mu}$ in the Appendix). These terms are often small and are typically ignored in adiabatic versions of FSSH. The FSSH results presented in Fig. 6 neglect these terms. Comparing results with our linearized schemes that include these terms suggest that they are indeed small and neglecting them is a good approximation for this model. More stringent test systems to study representation dependence of these different algorithms could be explored.[48]

D. Spin-boson model

We conclude Sec. III with a demonstration of the application of the various linearized and iterative density matrix propagation methods to the well studied spin-boson model of quantum dissipative dynamics in the condensed phase. Here we compare the performance of various approaches over a

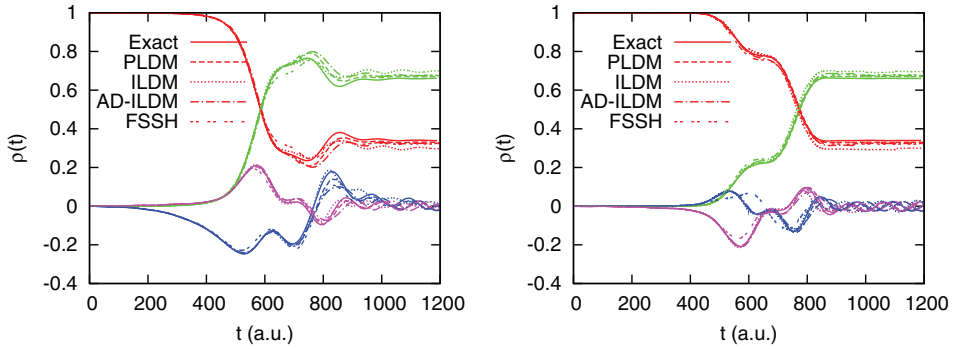

FIG. 6. Density matrix elements as functions of time for the Tully 2 dual avoided crossing Stueckelberg scattering model[1] with incident wave packet momentum $k = 30$ a.u. Here ρ_{11}, ρ_{22}, Re(ρ_{12}) and Im(ρ_{12}) are presented as red, green, blue, and magenta curves, respectively. The left panel compares results from different methods in the diabatic representation, while the right panel gives results in the adiabatic representation.

range of parameters including strength of system-bath coupling (Kondo parameter, solvent friction or reorganization energy), temperature, and energy bias between states. The results obtained with different approximate methods including: the PLDM propagation approach,[22] LANDmap,[21] ILDM,[24] LSC-IVR,[44] PEMB,[42] and TDSCF[4] methods are compared with exact path integral results.[49–51] Results obtained from LSC-IVR,[44] PBME[42] for the same type of model can be found in the cited references.

The spin-boson model involves a two state quantum subsystem (spin) bi-linearly coupled to a set of harmonic bath oscillators (bosons) defined by the following Hamiltonian:

$$\begin{aligned}\hat{H} &= \hat{H}_s + \hat{H}_b + \hat{H}_{s-b} \\ &= \epsilon\hat{\sigma}_z - \hbar\Omega\hat{\sigma}_x + \sum_j \left\{ \left[\frac{P_j^2}{2M_j} + \frac{1}{2}\omega_j^2 R_j^2 \right] \hat{1} - \hbar c_j R_j \hat{\sigma}_z \right\},\end{aligned} \tag{21}$$

where the $\hat{\sigma}_\alpha$ are the Pauli spin matrices, Ω is the strength of the electronic coupling between the diabatic states, ϵ is the relative off-set, or energy bias between the two diabatic spin states, (P_j, R_j) are the momentum and position of bath oscillator j, with frequency ω_j and c_j controls the strength of the bi-linear coupling between this bath oscillator and the quantum subsystem. The system-bath interactions in this model are specified by the model spectral density, $J(\omega)$, which determines the parameters c_j according to the following relationship: $J(\omega) = \frac{\pi}{2}\sum_j \frac{c_j^2}{M_j\omega_j}\delta(\omega - \omega_j)$. The spectral density is related to the thermal equilibrium correlation function of the diabatic site energy fluctuations driven by the bath according to the following expression: $\langle \sum_j c_j R_j(t) \sum_j c_j R_j(0)\rangle = \frac{\hbar}{\omega}\int_0^t d\omega J(\omega)[\coth(\hbar\beta\omega/2)\cos(\omega t) - i\sin(\omega t)]$. Here we choose units so that $\hbar = 1$ and use an ohmic spectral density at low frequencies (proportional to ω), with an exponential truncation at higher frequencies so in this model the spectral density has the form $J(\omega) = \frac{\pi}{2}\zeta\omega e^{-\omega/\omega_c}$, where ζ is the Kondo parameter (or friction, which determines the total interaction strength between system and bath) and ω_c is the cutoff, or peak frequency in this spectral density form. Here we use the exponential frequency sampling approach to generate bath frequencies and coupling strengths from this spectral density,[51] and the initial condition we use assumes the system is initially prepared in state 1 and the bath is in thermal equilibrium and the initially independent system-bath product density is employed, $\hat{\rho}(0) = \hat{\rho}_B|1\rangle\langle 1|$, where $\hat{\rho}_B$ is the Boltzmann operator for the independent harmonic oscillator bath.

In Fig. 7 we present typical results obtained with various methods for the symmetric spin-boson ($\epsilon = 0.0$) and the asymmetric spin-boson ($\epsilon \neq 0.0$) models. For the symmetric case we generally find that many of the different methods explored in our studies can reproduce the exact quantum results across a wide range of parameters. Panels (a)–(c) in Fig. 7 explore how the damped coherent population oscillations at low temperature, wash out more quickly as the temperature is increased and that the various approximate methods can capture these trends almost quantitatively. Similar quality results are generally found for the symmetric spin-boson if we scan a range of friction or environmental coupling strength.[21,24]

We generally find, however, that many of the approximate methods we have used in studies of this model encounter serious problems when we simply add an energy bias between the two spin states and consider the asymmetric spin boson model with $\epsilon \neq 0.0$. The LANDmap results presented in panel (d) of Fig. 7 typify the problem. With the LANDmap approach, where we linearize the density matrix propagator in the difference between forward and backward paths for all times, the short time behavior is reliable, but at long times the approach gives effectively infinite temperature results for which the two states, whose energies are different for the asymmetric spin-boson, have equal populations, so $\langle\hat{\sigma}_z\rangle$ has an unphysical infinite temperature value of zero at all temperatures. Other approximate methods such as the self-consistent classical path approach, some surface hopping techniques, and the Haken-Strobl model, for example, can all experience related problems when applied to study the long time approach to thermal equilibrium in this model.[4,52,53]

Results obtained when we iterate the linearized approach, using it as a short time approximation with the ILDM propagation method presented in Fig. 7(d), however, are seen to converge to the correct finite temperature limit at long times as we increase the number of iterations or "hops".[24] Reference 24 presents more detailed comparisons of results from ILDM propagation and other methods for the asymmetric spin boson and with exact wave packet calculations performed with the

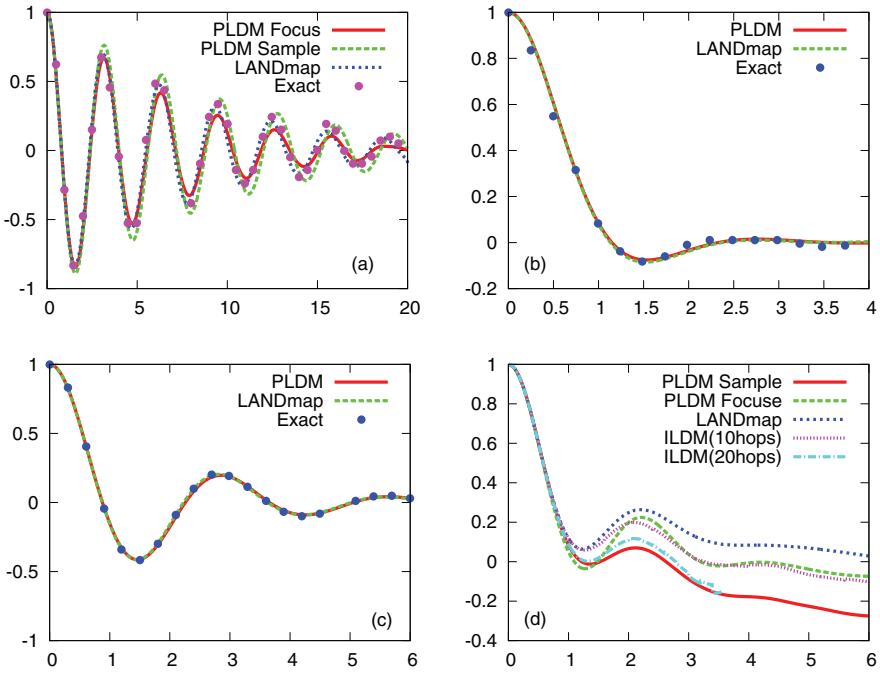

FIG. 7. Expectation value of population difference, $\langle\hat{\sigma}_z\rangle$, for the spin-boson model as a function of Ωt. Bottom right panel presents results for a system with state energy bias $\epsilon = 0.4$, all other present results for zero bias, $\epsilon = 0$. Top panels: $\Omega/\omega_c = 0.4$, $\zeta = 0.09$ with (a) top left $\beta\hbar\omega_c = 12.5$ and top right (b) $\beta\hbar\omega_c = 0.25$. (c) Bottom left: $\Omega/\omega_c = 0.4$, $\zeta = 0.13$, $\epsilon = 0$, $\beta\hbar\omega_c = 1$, and (d) Bottom right: has conditions the same as (c) except $\epsilon = 0.4$ and $\beta\hbar\omega_c$=1. Under the conditions used in panel (d) the thermal equilibrium value of $\langle\hat{\sigma}_z\rangle = -0.379$ is reproduced by the PLDM approach with sampled initial mapping variables.

multi-configuration time dependent Hartree (MCTDH) approach. These comparisons are conducted at very low temperatures ($\beta\hbar\omega_c = 12.5$) as the MCTDH wave packet propagation corresponds to zero temperature quantum dynamics. Our methods are easily applied at finite temperatures generally with little additional computational overhead, for example the results presented in Fig. 7(d) correspond to a higher temperature with $\beta\hbar\omega_c = 1.0$. In contrast, applying MCTDH at elevated temperatures requires Boltzmann averaging and can be prohibitively expensive.

The problem with general implementation of the ILDM approach is that it becomes extremely costly to perform the phase space integrations at intermediate iteration points. Also at longer times the noise in these ILDM calculations that arises from accumulating phase factors to capture interference effects for the off-diagonal density matrix elements becomes a serious problem for statistical convergence of the calculations and huge, prohibitive ensemble sizes are required. The dynamical population data compared in Fig. 7(d), however, suggest that when we can converge the ILDM propagation method, the results agree remarkably well with those obtained with the PLDM approach, which is observed to reliably capture the transition from short time coherent behavior to long time thermal equilibrium. The PLDM propagation approach typically requires thousands of times smaller ensembles to achieve statistical convergence of these highly accurate results.

From Fig. 7(d) we also see that the so-called "focusing" approximation,[24] which uses a steepest decent integration of the initial mapping variable distribution to improve numerical performance, can be unreliable when applied in concert with the PLDM propagation approach and that the full initial distribution must be sampled properly in order to obtain accurate results. The fully sampled PLDM propagation results presented in Fig. 7(d) also suggest that the approach converges to the expected classical-like behavior at long times and does not require exponentially increasing numbers of trajectories to achieve reliable long time results.

Finally, in Fig. 8 we explore the behavior of the linearized and iterated algorithms for the asymmetric spin-boson at low temperature where the quantum characteristics of the bath can in principle be significant. The left panel (a) shows the population relaxation computed using the mean-field PLDM and iterated IPLMD version of the approach. The right panel (b) gives results from a similar study using the state dependent force LANDmap approach and shows how it converges with increasing number of iterations. The exact results presented here are obtained with zero temperature MCTDH calculations. The temperature used in our studies corresponding to $\beta\hbar\omega_c = 12.5$, where $\beta = 1/k_BT$, is sufficiently low that this comparison with zero temperature exact results is reliable.

In the right panel (b) we see that the basic LANDmap approach behaves like an infinite temperature theory, it captures some aspects of the short time coherent dynamics but fails to give long time thermal equilibration in that the long time population difference tends, unphysically, to zero for this asymmetric two state model. As the algorithm is iterated using the LANDmap propagator as a short time propagator, however, we see that the population difference begins to converge to the exact results, which have a negative value for the thermal expectation, $\langle\sigma_z\rangle$, due to the strong asymmetry in this model. We see that for this problem many short time LANDmap propagations are requires to achieve convergence on the exact result, however, with such a large number of iterations required, the

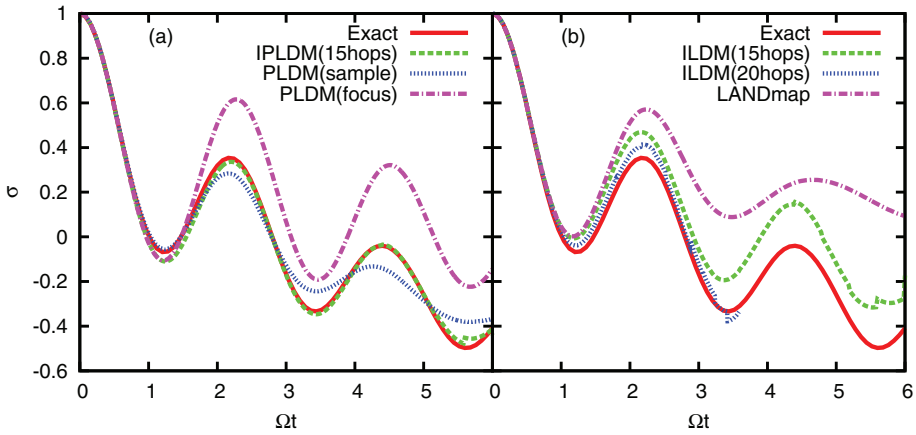

FIG. 8. $\langle\sigma_z(t)\rangle$ versus Ωt for spin-boson model, with $\Omega/\omega_c = 0.4$, $\zeta = 0.13$, $\epsilon = 0.4$, $\beta\hbar\omega_c = 12.5$. (a) Left panel gives results obtained with linearized and iterative algorithms based on the PLDM approximate short time propagator. (b) Right panel shows results obtained using LANDmap approximate short time propagator as the basis of iteration. In each panel results are explored as a function on the number of iterations.

statistical noise at longer times becomes prohibitive. The discontinuous jumps observed in the data mark the boundaries of successive time slices. With in a time slice we average segments of smooth functions, but between adjacent slices these averages have not yet converged at the longer times so the data shows jumps between segments of poorly statistically converged averages.

The left panel (a) of Fig. 8 demonstrates the significantly superior convergence properties of the PLDM propagator for these types of models. We see that the basic PLDM propagator with sampled initial conditions captures both the coherent oscillatory features and the correct long time thermal equilibrium behavior of the asymmetric model requiring no iteration. The coherent oscillation is slightly over damped compared to the exact results but generally the basic short time propagator give qualitatively reliable results for the entire duration of the propagation. When focused initial conditions are used, not surprisingly, the coherent oscillatory behavior is enhanced and the system relaxes a little too slowly. On iterating this short time approximate propagator we see that it rapidly converges to give quantitative agreement with the exact results with as few as 15 iterations (hops), and the statistical errors are significantly reduced compared to the results found for ILDM propagation.

IV. CONCLUDING REMARKS

We have demonstrated that alternative approximate nuclear trajectory based non-adiabatic quantum dynamics algorithms can be derived by applying the partial linearization approach to a full path integral expression for density matrix propagation in different ways. These different algorithms can provide reliable short time approximate propagation that can, in principle, be applied to treat general large scale complex system quantum dynamics. We have also presented a viable iterative implementation of these short time approximate propagators that enables accurate long time quantum propagation. This iteration procedure, however, requires making additional approximations to the intermediate integrations over the initial conditions for each time slice.

The short time approximate propagators that we have found from these different approaches to linearization produce forces on the classical-like nuclear degrees of freedom that either resemble those appearing in the mean-field Ehrenfest treatments (e.g., our short time PLDM propagator), or instantaneous quantum subsystem "state" dependent forces like those of trajectory based surface hopping schemes (e.g., our short time LANDmap propagator).

The important simplifying feature of the partial linearization approach is that because we work with density matrix propagation we can approximately combine parts of the highly oscillatory phase factors of the forward and backward propagators, in particular, partial linearization combines the forward and backward nuclear phase factors to approximate the path integral kernel as a product of δ-functions that identify classical nuclear trajectory-like equations of motion. The remaining electronic subsystem phase factors and weights are carried along by the trajectories that result from this partial linearization. Coherently combining the weights and phases of each of these trajectories presents a significant numerical challenge for our scheme. Our successful calculations of the non-adiabatic bifurcating nuclear momentum distributions presented in Sec. III A, however, demonstrate that these approximate methods can be applied to reliably capture sensitive phase interference effects. Preliminary studies exploring the use of energy conserving momentum jumps to mimic the effects of these interference phenomena are very promising and represent an important next step towards deriving a rigorous, efficient, and reliable way to treat such processes beyond the adoption of *ad hoc* rules that plague many surface hopping implementations.

The studies outlined here suggest that the iterative implementations of our PLDM and LANDmap short time approximate propagators, the IPLDM and ILDM methods, respectively, have different numerical scaling. With the LANDmap propagator, for example, in order to evolve all the density matrix elements, $n(n+1)/2$ different trajectories each experiencing different state dependent forces must be evolved in order to make our decision about which density matrix states will be initiated in the next time slice using our Monte Carlo

importance sampling approach. With the mean-field PLDM based approach, on the other hand, all the density matrix elements are generated with a trajectory integrated using a single mean force so the PLDM propagation is in principle of order $\mathcal{O}(n^2)$ times more efficient than the LANDmap based propagation procedure. It also appears that the PLDM short time propagator may, in some situations, provide more accurate propagation for longer times, thus reducing the number of iterations needed for long time propagation.

As a final point we note that in the framework of the MQCL equation, one can also achieve either a surface hopping-like approach[27,30] in the adiabatic representation using a Trotter-based approximate propagation scheme and Monte Carlo sampling, or a mean-field like algorithm in a diabatic representation using the mapping Hamiltonian formalism.[42] Given the fact that MQCL equation propagation can also be derive from a linearization approximation,[54] it is not surprising that the linearized path integral methods and the MQCL propagation schemes can yield similar classes of algorithms. The relationship between these formulations is further explored in the recent publication by Kapral and co-workers that appears in this issue.[55]

ACKNOWLEDGMENTS

We gratefully acknowledge support for this research from the National Science Foundation (NSF) under Grant No. CHE-0911635 and support from Science Foundation Ireland under Grant No 10/IN.1/I3033. D.F.C. acknowledges the support of his Stokes Professorship in Nanobiophysics from Science Foundation Ireland. We also acknowledge a grant of supercomputer time from Boston University's Office of Information Technology and Scientific Computing and Visualization. Finally, we would like to thank John Tully for inspiring our work in this area.

APPENDIX: ADIABATIC REPRESENTATION MAPPING THEORY

In this appendix we summarize an adiabatic version of the state dependent force ILDM algorithm, the details of which can be found in Ref. 26. We begin by representing the total wave function in a basis chosen as the tensor product of the nuclear coordinates $|R\rangle$ and the adiabatic electronic basis set, i.e., $|\Psi_\lambda(R)\rangle$ such that

$$\hat{h}_{el}|\Psi_\lambda(R)\rangle = E_\lambda(R)|\Psi_\lambda(R)\rangle. \tag{A1}$$

The total Hamiltonian in this representation is obtained as

$$\hat{H} = \frac{\hat{P}_\chi^2}{2M} + \sum_{\lambda,\mu} |\Psi_\lambda(R)\rangle (E_\lambda(R)\delta_{\lambda,\mu} + \hat{\Lambda}_{\lambda,\mu}(R))\langle\Psi_\mu(R)|, \tag{A2}$$

where

$$\hat{\Lambda}_{\lambda,\mu}(R) = -\left[i D_{\lambda,\mu}(R)\frac{\hat{P}_\chi}{M} + \frac{1}{2M} G_{\lambda,\mu}(R)\right], \tag{A3}$$

with

$$\begin{aligned} D_{\lambda,\mu}(R) &= \langle\Psi_\lambda(R)|\frac{\partial}{\partial R}|\Psi_\mu(R)\rangle, \\ G_{\lambda,\mu}(R) &= \langle\Psi_\lambda(R)|\frac{\partial^2}{\partial R^2}|\Psi_\mu(R)\rangle. \end{aligned} \tag{A4}$$

This Hamiltonian acts on a general vibronic wave function of the form $|\Phi\rangle = \sum_\mu \chi_\mu(R)|\Psi_\mu(R)\rangle$ were $\chi_\mu(R)$ is the nuclear coefficient function. Note that $\hat{\Lambda}$ is an operator in $\hat{P}_\chi$ and a function of the nuclear coordinates. The differential operator $\hat{P}_\chi = i\frac{\partial}{\partial R}$ acts on the nuclear coefficient functions, $\chi_\mu(R)$, only, i.e., it does not touch the parametric dependence on R of the adiabatic wave functions. $D_{\lambda,\mu}(R)$ is known as the non-adiabatic coupling vector and together with the other non Born-Oppenheimer term, $G_{\lambda,\mu}(R)$, is responsible for the non-adiabatic transitions.

The $\hat{h}_{el}$ part of the adiabatic representation Hamiltonian in Eq. (A2) can be written applying the mapping formalism as follows:

$$\begin{aligned} \hat{h}_{map} = &\frac{1}{2}\sum_\lambda E_\lambda(R)\left(\hat{q}_\lambda^2 + \hat{p}_\lambda^2 - 1\right) \\ &+ \frac{1}{2}\sum_{\lambda\mu} Re\hat{\Lambda}_{\lambda\mu}(R)(\hat{q}_\lambda\hat{q}_\mu + \hat{p}_\lambda\hat{p}_\mu - \delta_{\lambda\mu}) \\ &- \frac{1}{2}\sum_{\lambda\mu} Im\hat{\Lambda}_{\lambda\mu}(R)(\hat{q}_\lambda\hat{p}_\mu - \hat{p}_\lambda\hat{q}_\mu). \end{aligned} \tag{A5}$$

In deriving the equation above, we have used the fact that $\Lambda_{\lambda\mu} = \Lambda^*_{\mu\lambda}$.

Following a similar semi-classical argument to that in Ref. 21, one can cancel[26] the analogous pre factor term, c_t, with the $-1/2(E_\lambda - Re\Lambda_{\lambda\lambda})$ diagonal terms in Eq. (A5), which again solves the problem of trajectories moving on the inverted potential. Proceeding as above we again introduce the action and angle variables,

$$\Theta_{t,\beta}(\{R_k\}) = \tan^{-1}\left(\frac{p_{0,\beta}}{q_{0,\beta}}\right) + \int_0^t d\tau\left[\theta_{\tau,\beta} + \frac{\hat{P}_\chi}{M}W_{\tau,\beta}\right], \tag{A6}$$

where

$$\begin{aligned} \theta_{\tau,\beta} = &-[E_\beta(R_\tau) - Re\Lambda_{\beta\beta}(R_\tau)] \\ &- \sum_{\lambda(\neq\beta)}\left[Re\Lambda_{\beta,\lambda}(R_\tau)\frac{(p_{\tau\beta}p_{\tau\lambda} + q_{\tau\beta}q_{\tau\lambda})}{(p_{\tau\beta}^2 + q_{\tau\beta}^2)}\right], \end{aligned} \tag{A7}$$

and

$$W_{\tau,\beta} = \sum_{\lambda(\neq\beta)}\left[D_{\beta\lambda}(R_t)\frac{(p_{\tau\lambda}q_{\tau\beta} - p_{\tau\beta}q_{\tau\lambda})}{(p_{\tau\beta}^2 + q_{\tau\beta}^2)}\right]. \tag{A8}$$

We incorporate the nuclear momentum containing $W_{\tau,\beta}\hat{P}_\chi/M$ term into the nuclear kinetic action, to obtain[26]

$$S_P = \epsilon\sum_k\left\{P_k\frac{(R_{k+1} - R_k)}{\epsilon} - \frac{1}{2M}[P_k + W_\beta]^2\right\}. \tag{A9}$$

The partial linearized approximation for the nuclear DOF then gives the final expression within the state dependent force

ILDM propagation formulation as

$$\begin{aligned}
&\rho_{n_t,n_t'}(\bar{R},t)\\
&=\sum_{n_0,n_0'}\int d\bar{R}_0 dq_0 dp_0 dq_0' dp_0' \int\prod_{k=1}^{N} d\bar{R}_k \frac{d\bar{P}_k}{2\pi}\\
&\times(\hat{\rho})_W^{n_0,n_0'}(\bar{R}_0,\bar{P}_1)e^{-i\Omega}G_0G_0'r_{0,n_0}e^{i\theta_{0,n_0}}\tilde{r}_{0,n_0'}e^{-i\theta'_{0,n_0'}}\\
&\times r_{t,n_t}(\{\bar{R}_k\})r'_{t,n_t'}(\{\bar{R}_k\})e^{\frac{i}{\hbar}(\bar{P}_N-\Pi_N^{n_t,n_t'}/M)Z_N}\\
&\times\prod_{k=1}^{N-1}\delta\left(\frac{\bar{P}_{k+1}-\bar{P}_k}{\epsilon}-F_k^{n_t,n_t'}\right)\\
&\times\prod_{k=1}^{N}\delta\left(\frac{\bar{R}_k-\bar{R}_{k-1}}{\epsilon}-\frac{\Pi_k^{n_t,n_t'}}{M}\right),
\end{aligned}\tag{A10}$$

where the force $F_k^{n_t,n_t'}$ that acts on nuclear coordinate is obtained as

$$\begin{aligned}
F_k^{n_t,n_t'}=&-\frac{1}{2M}\bar{P}_k\nabla_{\bar{R}_k}(W_{n_t}(\bar{R}_k)+W'_{n_t'}(\bar{R}_k))\\
&-\frac{1}{2M}(W_{n_t}\nabla_{\bar{R}_k}W_{n_t}+W'_{n_t'}\nabla_{\bar{R}_k}W'_{n_t'})\\
&-\frac{1}{2}\nabla_{\bar{R}_k}(\theta_{n_t}(\bar{R}_k)+\theta'_{n_t'}(\bar{R}_k)),
\end{aligned}\tag{A11}$$

and the momentum term $\Pi_k^{n_t,n_t'}$ contains a "momentum jump" contribution due to the non-adiabatic coupling factor so that

$$\Pi_k^{n_t,n_t'}=\left[\bar{P}_k+\frac{W_{n_t}(\bar{R}_{k-1})+W'_{n_t'}(\bar{R}_{k-1})}{2}\right].\tag{A12}$$

Also, there is an additional phase factor $e^{-i\Omega}$ in this expression that comes from the zeroth order term of the partial linearization in difference between forward and backward nuclear paths. Here $\Omega=\epsilon\{\sum_k\frac{\bar{P}_k}{M}[W_{n_t}(\bar{R}_k)-W'_{n_t'}(\bar{R}_k)]+\frac{1}{2M}[W_{n_t}^2(\bar{R}_k)-W'^{\,2}_{n_t'}(\bar{R}_k)]+[\theta_{n_t}(\bar{R}_k)-\theta'_{n_t'}(\bar{R}_k)]\}$.

The main difference between the linearized approaches in the adiabatic and diabatic representations lies in the structure of the evolution equations for the bath degrees of freedom. In the adiabatic picture, the force is not simply the gradient of a function of the nuclear coordinates times a term that depends on the mapping variables. Rather, it contains a multiplicative coupling of the "potential" to the momenta, in close analogy to the classical evolution equations of a charged particle moving in a magnetic field,[56] and Brownian motion.[39,56] The analogy is particularly evident in the form of the action in Eq. (A9), where W plays the role of a vector potential.[57]

We should also point out that, Miller and co-workers have obtained a similar result for the mapping Hamiltonian in adiabatic representation,[10,43] however, instead of the term $\langle\Psi_\lambda(R)|\frac{\partial^2}{\partial R^2}|\Psi_\mu(R)\rangle$ obtained from the development outlined above, their second order term is actually $\langle\Psi_\lambda(R)|\frac{\partial}{\partial R}|\Psi_\mu(R)\rangle^2$. This is because they follow a quite different route of the derivation by exploiting the correspondence between the similarity transformation leading from one basis set to another in quantum mechanics and a classical canonical transformation, to derive a form for the evolution equations in the adiabatic basis after taking the semi-classical limit for the propagator in the diabatic mapping representation. On the other hand, we start from a exact quantum expression, then use the mapping formalism.

This adiabatic version of LANDmap can also be extend to longer times by applying the short time linearized approximation iteratively as outlined above. Again, combining the boundary terms from two adjacent segments, $e^{\frac{i}{\hbar}(\bar{P}_N-\Pi_N^{n_t,n_t'}/M)Z_N}$ and $e^{-\frac{i}{\hbar}(\bar{P}_{N+1}-\Pi_{N+1}^{n_t,n_t'}/M)Z_N}$, and integrating out the path difference we obtain a connection condition from one segment to the next, $\delta(\bar{P}_{N+1}-\bar{P}_N+[\Pi_N^{n_t,n_t'}/M-\Pi_{N+1}^{n_t,n_t'}/M])$, which provides a momentum jump term. We can also derive a mean-field version of the adiabatic theory following a similar procedure to that outlined above for iterating the PLDM approach. The final result of this development will be a mean-field force that is the derivative of the classical adiabatic Hamiltonian.

[1] J. C. Tully, J. Chem. Phys. **93**, 1061 (1990); in *Classical and Quantum Dynamics in Condensed Phase Simulations*, edited by G. Ciccotti, B. Berne, and D. Coker (World Scientific, Dordrecht, 1998), p. 489.
[2] G. Stock and M. Thoss, "Mixed quantum-classical description of the dynamics at conical intersections," in *Conical Intersections*, edited by W. Domcke, D. R. Yarkony, and H. Köppel (World Scientific, Singapore, 2003).
[3] P. Pechukas, Phys. Rev. **181**, 174 (1969).
[4] G. Stock, J. Chem. Phys. **103**, 1561 (1995).
[5] D. F. Coker and X. Li, J. Chem. Phys. **102**, 496 (1995).
[6] U. Müller and G. Stock, J. Chem. Phys. **107**, 6230 (1997).
[7] N. Shenvi, J. E. Subotnik, and W. Yang, J. Chem. Phys. **135**, 024101 (2011); **134**, 144102 (2011).
[8] Y. Wu and M. F. Herman, J. Chem. Phys. **123**, 144106 (2005); **125**, 154116 (2006).
[9] X. Sun, H. Wang, and W. H. Miller, J. Chem. Phys. **109**, 7064 (1998).
[10] N. Ananth, C. Venkataraman, and W. H. Miller, J. Chem. Phys. **127**, 084114 (2007).
[11] B. R. Landry and J. E. Subotnik, J. Chem. Phys. **135**, 191191 (2011); J. E. Subotnik and N. Shenvi, *ibid.* **134**, 244114 (2011); N. Shenvi, and J. E. Subotnik, *ibid.* **134**, 024105 (2011).
[12] The accurate adiabatic population, can only be obtained from the "binned" coefficients that count the fraction of trajectories in a particular state. The actual electronic coefficients obtained from the evolution of time dependent Schördinger equation, however, do not give same population as the binned coefficients and generally give an inaccurate picture of the evolution of the adiabatic populations.[2]
[13] S. Hammes-Schiffer and J. C. Tully, J. Chem. Phys. **101**, 4657–4667 (1994).
[14] Y. Volobev, M. D. Hack, M. S. Topaler, and D. G. Truhlar, J. Chem. Phys. **112**, 9716 (2000); M. D. Hack, and D. G. Truhlar, J. Phys. Chem. A **104**, 7917 (2000).
[15] O. Prezhdo and P. J. Rossky, J. Chem. Phys. **107**, 825 (1997).
[16] S. A. Fischer, C. T. Chapman, and X. Li, J. Chem. Phys. **135**, 144102 (2011).
[17] J. Bader and B. Berne, J. Chem. Phys. **100**, 8359 (1994); B. Berne, J. Bader, and P. Hanggi, *ibid.* **104**, 1111 (1996); S. Egorov, E. Rabani, and B. Berne, J. Phys. Chem. A **103**, 10978 (1999).
[18] P. V. Parandekar and J. C. Tully, J. Chem. Phys. **122**, 094102 (2005); J. Chem. Theory. Comput. **2**, 229 (2006).
[19] H. D. Meyer and W. H. Miller, J. Chem. Phys. **70**, 3214 (1979); G. Stock and M. Thoss, Phys. Rev. Lett. **78**, 578 (1997); M. Thoss and G. Stock, Phys. Rev. A **59**, 64 (1999).
[20] Q. Shi and E. Geva, J. Chem. Phys. **121**, 3393 (2004); Q. Shi and E. Geva, J. Phys. Chem. A **108**, 6109 (2004).
[21] S. Bonella and D. F. Coker, J. Chem. Phys. **122**, 194102 (2005); S. Bonella, D. Montemayor and D. F. Coker, Proc. Natl. Acad. Sci. U.S.A. **102**, 6715 (2005).
[22] P. Huo and D. F. Coker, J. Chem. Phys. **135**, 201101 (2011).
[23] P. Huo and D. F. Coker, Mol. Phys. **110**, 1035 (2012).

[24]E. R. Dunkel, S. Bonella, and D. F. Coker, J. Chem. Phys. **129**, 114106 (2008).
[25]S. Bonella and D. F. Coker, J. Chem. Phys. **118**, 4370 (2003).
[26]S. Bonella and D. F. Coker, in *Quantum Dynamics of Complex Molecular Systems*, Lectures in Chemical Physics Vol. 83, edited by D. Micha and I. Burghardt (Springer, Berlin, 2006), p. 321.
[27]D. Mac Kernan, G. Ciccotti, and R. Kapral, J. Chem. Phys. **116**, 2346 (2002); J. Phys. Chem. B **112**, 424 (2008).
[28]E. A. Coronado, J. Xing, and W. H. Miller, Chem. Phys. Lett. **349**, 512 (2001).
[29]S. Bonella and D. F. Coker, J. Chem. Phys. **114**, 7778 (2001).
[30]A. Kelly, R. van Zon, J. Schofield, and R. Kapral, J. Chem. Phys. **136**, 084101 (2012).
[31]G. Tao and W. H. Miller, J. Phys. Chem. Lett. **1**, 891 (2010).
[32]U. Müller and G. Stock, J. Chem. Phys. **111**, 77 (1999).
[33]J. A. Poulsen, G. Nyman, and P. J. Rossky, J. Chem. Phys. **119**, 12179 (2003); Q. Shi and E. Geva, *ibid.* **118**, 8173 (2003).
[34]J. Vanicek, Phys. Rev. E **70**, 055201(R) (2004).
[35]N. Ananth and T. F. Miller III, J. Chem. Phys. **133**, 234103 (2010); Z. Ma and D. F. Coker, *ibid.* **128**, 244108 (2008).
[36]The idea of focusing[25] is, instead of sampling the initial conditions for the mapping variables, we can find the steepest descent points of integrations over these variables by optimizing the integrand $\frac{1}{4}(q_{n_0}+ip_{n_0})(q_{n_0}-ip_{n_0})e^{-\frac{1}{2}\sum_\beta(q_{\beta 0}^2+p_{\beta 0}^2)}$ is $q_{n_0}^2+p_{n_0}^2=2$, with similar for the backward mapping variables, and simply these single points in mapping variable phase space. So the idea is to replace the sampling of the gaussian distribution of the mapping variable $e^{-\frac{1}{2}\sum_\beta(q_{\beta 0}^2+p_{\beta 0}^2)}$ as a delta function $\delta(\{q_{n_0}^2+p_{n_0}^2\}-2)$ by this single point approximation.
[37]U. Müller and G. Stock, J. Chem. Phys. **108**, 7516 (1998).
[38]P. Huo and D. F. Coker, J. Chem. Phys. **133**, 184108 (2010).
[39]P. Huo, S. Bonella, L. Chen, and D. F. Coker, Chem. Phys. **370**, 87 (2010).
[40]W. H. Miller and C. W. McCurdy, J. Chem. Phys. **69**, 5163 (1978); C. W. McCurdy, H. D. Meyer, and W. H. Miller, *ibid.* **70**, 3177 (1979).
[41]E. Martin-Fierro and E. Pollak, J. Chem. Phys. **126**, 164108 (2007).
[42]H. Kim, A. Nassimi, and R. Kapral, J. Chem. Phys. **129**, 084102 (2008); A. Nassimi and R. Kapral, Can. J. Chem. **87**, 880 (2009).
[43]X. Sun and W. H. Miller, J. Chem. Phys. **106**, 6346 (1997).
[44]H. Wang, X. Song, D. Chandler, and W. H. Miller, J. Chem. Phys. **110**, 4828 (1999).
[45]H. Wang, M. Thoss, K. L. Sorge, R. Gelabert, X. Giménez, and W. H. Miller, J. Chem. Phys. **114**, 2562 (2001).
[46]J. Subotnik, J. Chem. Phys. **132**, 134112 (2010).
[47]G. Tao and W. H. Miller, J. Chem. Phys. **130**, 184108 (2009).
[48]J. Tully, Faraday Discuss. **110**, 407 (1998).
[49]D. E. Makarov and N. Makri, Chem. Phys. Lett. **221**, 482 (1994).
[50]R. Egger and C. H. Mak, Phys. Rev. B **50**, 15210 (1994).
[51]K. Thompson and N. Makri, J. Chem. Phys. **110**, 1343 (1999).
[52]A. Ishizaki and G. R. Fleming, J. Phys. Chem. B **115**, 6227 (2011).
[53]X. Chen and R. J. Silbey, J. Chem. Phys. **132**, 204503 (2010).
[54]S. Bonella, G. Ciccotti, and R. Kapral, Chem. Phys. Lett. **484**, 399 (2010).
[55]C.-Y. Hsieh and R. Kapral, J. Chem. Phys. **137**, 22A507 (2012).
[56]L. S. Shulman, *Techniques and Applications of Path Integration* (Wiley, New York, 1981).
[57]This structure does not come as a surprise, since it is a direct consequence of the nature of the non-adiabatic coupling in the chosen basis. Quantum mechanically, transitions among different electronic states are governed by the operator $\hat{\Lambda}_{\lambda\mu}$, introduced in Eq. (A3), that contains the same kind of coupling between the nuclear momentum and position operators.